



1

2

3 **Investigating basin-scale water budget dynamics in 18 rivers across**
4 **Tibetan Plateau through multiple datasets**

5 Wenbin Liu^a, Fubao Sun^{a,b,*}, Yanzhong Li^a, Guoqing Zhang^{c,d}, Yan-Fang Sang^a,

6 Wee Ho Lim^{a,e}, Jiahong Liu^f, Hong Wang^a, Peng Bai^a

7

8 ^aKey Laboratory of Water Cycle and Related Land Surface Processes, Institute of Geographic
9 Sciences and Natural Resources Research, Chinese Academy of Sciences, Beijing 100101, China

10 ^bHexi University, Zhangye 734000, China ^cKey Laboratory of Tibetan Environmental Changes
11 and Land Surface Processes, Institute of Tibetan Plateau Research, Chinese Academy of Sciences,
12 Beijing 100101, China ^dCAS Center for Excellent in Tibetan Plateau Earth Sciences, Beijing

13 100101, China ^eEnvironmental Change Institute, Oxford University Centre for the Environment,
14 School of Geography and the Environment, University of Oxford, Oxford OX1 3QY, UK ^fKey
15 Laboratory of Simulation and Regulation of Water Cycle in River Basin, China Institute of Water
16 Resources and Hydropower Research, Beijing 100038, China

17

18

19 **Corresponding Author:** Dr. Fubao Sun (Sunfb@igsnr.ac.cn), Key Laboratory of Water Cycle
20 and Related Land Surface Processes, Institute of Geographic Sciences and Natural Resources
21 Research, Chinese Academy of Sciences

22

23



Abstract The dynamics of basin-scale water budgets are not well understood nowadays over the Tibetan Plateau (TP) due to the lack of hydro-climatic observations. In this study, we investigate seasonal cycles and trends of water budget components (e.g., precipitation-P, evapotranspiration-ET and runoff-Q) in eighteen TP river basins during the period 1982-2011 through the use of multi-source datasets (e.g., in situ observations, satellite retrievals, reanalysis outputs and land surface model simulations). A water balance-based two-step procedure, which considers the changes in basin-scale water storage at the annual scale, is also adopted to calculate actual ET. The results indicated that precipitation (mainly snowfall from mid-autumn to next spring), which mainly concentrated during June-October (varied among different monsoons-impacted basins), was the major contributor to the runoff in TP basins. Increased P, ET and Q were found in most TP basins during the past 30 years except for the upper Yellow River basin and some sub-basins of Yalong River, which were mainly affected by the weakening East Asian Monsoon. Moreover, the aridity index (PET/P) and runoff coefficient (Q/P) decreased in most basins, which were in agreement with the warming and moistening climate in the Tibetan Plateau. The results obtained demonstrated the usefulness of integrating multi-source datasets to hydrological applications in the data-sparse regions. More generally, such approach might offer helpful insights towards understanding the water and energy budgets and sustainability of water resource management practices of data-sparse regions in a changing environment.



46 **1 Introduction**

47 As the highest plateau in the globe (the average elevation is higher than 4000 meters
48 above the sea level), the Tibetan Plateau (TP, also called “the roof of the world” or
49 “the third Pole”) is regarded as one of the most vulnerable regions under a warming
50 climate and is exposed to strong interactions among atmosphere, hydrosphere,
51 biosphere and cryosphere in the earth system (Duan and Wu, 2006; Yao et al., 2012;
52 Liu et al., 2016b). It also serves as the “Asian water tower” from which some major
53 Asian rivers such as Yellow River, Yangtze River, Brahmaputra River, Mekong River,
54 Indus River, etc., originate, which is a vital water resource to support the livelihood of
55 hundreds of millions of people in China and the neighboring Asian countries
56 (Immerzeel et al., 2010; Zhang et al., 2013). Hence sound knowledge of water budget
57 and hydrological regimes in TP river basins and its response to the changing
58 environment would have practical relevance for achieving sustainable water resource
59 management and environmental protection in this part of the world (Yang et al., 2014;
60 Chen et al., 2015).

61
62 Despite the importance of TP in this geographic region, advance in hydrological and
63 land surfaces studies in this region has been limited by data scarcity (Zhang et al.,
64 2007; Li F. et al., 2013; Liu X. et al., 2016). For instance, less than 80 observation
65 stations (~10% of a total of ~750 observation station across China) have been
66 established in TP by the Chinese Meteorological Administration (CMA) since the
67 mid-20th century (Wang and Zeng, 2012). These stations are generally sparse and
68 unevenly distributed at relatively low elevation regions, focus only on the
69 meteorological variables and lack of other land surface observations such as
70 evapotranspiration, snow water equivalent and latent heat fluxes. In addition,



71 long-term observations of river discharge, snow depth, lake depth and glacier melts in
72 the TP are also absent (Akhta et al., 2009; Ma et al., 2016). Therefore, the water
73 budget and hydrological regimes for each river basin of TP and their relation with
74 atmospheric circulations are poorly understood (Cuo et al., 2014; Xu et al., 2016).
75 Whilst this shortcoming could be resolved through installation of in-situ monitoring
76 systems (Yang et al., 2013; Zhou et al., 2013; Ma et al., 2015), the overall cost of
77 running the operational sites would be substantial. Another workaround would be
78 through modeling approach, i.e., feeding remote sensing information and
79 meteorological forcing data into physically-based land surface model (LSM) to
80 simulate the basin-wide water budget (Bookhagen and Burbank, 2010; Xue et al.,
81 2013; Zhang et al., 2013; Cuo et al., 2015; Zhou et al., 2015; Wang et al., 2016).
82 However, such approach is not immune from the issue of data scarcity at multiple
83 river basins (with varied sizes and/or terrain complexities) for supporting model
84 calibration and validation purposes (Li F. et al., 2014).
85
86 Most recently, several global (or regional) datasets relevant to the calculation of water
87 budget have been released. They include remote sensing-based retrievals (Tapley et al.,
88 2004; Zhang et al., 2010; Long et al., 2014; Zhang Y. et al., 2016), land surface model
89 (LSM) simulations (Rui, 2011), reanalysis outputs (Berrisford et al., 2011; Kobayashi
90 et al., 2015) and gridded forcing data interpolated from the in situ observations
91 (Harris et al., 2014). For example, there are many products related to terrestrial
92 evapotranspiration (ET) such as GLEAM_E (Global Land surface Evaporation: the
93 Amsterdam Methodology, Miralles et al., 2011a), MTE_E (a product integrated the
94 point-wise ET observation at FLUXNET sites with geospatial information extracted
95 from surface meteorological observations and remote sensing in a machine-learning



96 algorithm, Jung et al., 2010), LSM-simulated ETs from Global Land Data
97 Assimilation System version 2 (GLDAS-2) with different land surface schemes
98 (Rodell et al., 2004), ETs from Japanese 55-year reanalysis (JRA55_E), the
99 ERA-Interim global atmospheric reanalysis dataset (ERA-Interim) and the National
100 Aeronautic and Space Administration (NASA) Modern Era Retrospective-analysis
101 for Research and Application (MERRA) reanalysis data (Lucchesi, 2012). Moreover,
102 there are also several global or regional LSM-based runoff simulations from GLDAS
103 and the Variable Infiltration Capacity (VIC) model (Zhang et al., 2014). A few
104 attempts have been made to validate multiple datasets for certain water budget
105 components and to explore their possible hydrological implications. For example, Li
106 X. et al. (2014) and Liu et al. (2016a) evaluated multiple ET estimates against the
107 water balance method at annual and monthly time scales. Bai et al. (2016) assessed
108 streamflow simulations of GLDAS LSMs in five major rivers over the TP based on
109 the discharge observations. Although uncertainties might exist among different
110 datasets with various spatial and temporal resolutions and calculated using different
111 algorithms (Xia et al., 2012), they offer an opportunity to examine the general
112 basin-wide water budgets and their uncertainties in gauge-sparse regions such as the
113 TP considered in this study.

114

115 From the multiple datasets perspective, this study aims to investigate the water budget
116 in 18 TP river basins distributed across the Tibetan Plateau; and evaluate seasonal
117 cycles and annual trends of these water budget components. This paper is organized
118 as follows: the datasets and methods applied in this study are described in Sect.2. The
119 results of season cycles and annual trends of water budget components for the river
120 basins are presented and discussed in Sect.3. The uncertainties arise from employing



multiple datasets are also discussed in the same section. In Sect.4, we generalize our findings which would be helpful for understanding the water balances of the river basins under constant influence of interplay between westerlies and monsoons (e.g., Indian monsoon, East Asian monsoon) in the Tibetan Plateau.

125

2 Data and methods

2.1 Multiple datasets used

2.1.1 Runoff, precipitation and terrestrial storage change

We obtained the observed daily runoff (Q) during the period 1982-2011 from the National Hydrology Almanac of China (Table 1). There are < 30% missing data in some gauging stations such as Yajiang, Tongren, Gandatan and Zelingou. Therefore, the VIC Retrospective Land Surface Dataset over China (1952~2012, VIC_IGSNRR simulated) with a spatial resolution of 0.25 degree and a daily temporal resolution from the Geographic Sciences and Natural Resources Research (IGSNRR), Chinese Academy of Sciences, is also used. This dataset is derived from the VIC model forced by the gridded daily observed meteorological forcing (IGSNRR_forcing) (Zhang et al., 2014). A degree-day scheme was used in the model to account for the influences of snow and glacier on hydrological processes.

139

In terms of precipitation (P), we used the gridded monthly precipitation dataset available at CMA (spatial resolution of 0.5 degree; 1961-2011; interpolated from observations of 2372 national meteorological stations using the Thin Plate Spline method) (Table 1). Since the reliability of this dataset might be restricted by the relatively sparse stations and complex terrain conditions of TP, we make an attempt to incorporate two other precipitation datasets ((IGSNRR_forcing and Tropical Rainfall



146 Measuring Mission TRMM 3B43 V7). The precipitation from IGSNRR forcing
147 datasets (0.25 degree) was derived by interpolating gauged daily precipitation from
148 756 CMA stations based on the synergraphic mapping system algorithm (Shepard,
149 1984; Zhang et al., 2014) and was further bias-corrected using the CMA gridded
150 precipitation.

151

152 To get the change in terrestrial storage (ΔS), we used three latest global terrestrial
153 water storage anomaly and water storage change datasets (available on the GRACE
154 Tellus website: <http://grace.jpl.nasa.gov/>) that were retrieved from the Gravity
155 Recovery and Climate Experiment (GRACE, Tapley et al., 2004; Landerer and
156 Swenson, 2012; Long et al., 2014). Briefly, they were processed separately at the Jet
157 Propulsion Laboratory (JPL), the GeoForschungsZentrum (GFZ) and the Center for
158 Space Research at the University of Texas (CSR). To minimize the errors and
159 uncertainty of extracted ΔS , we averaged these GRACE retrievals (2002-2013) from
160 different processing centers in this study.

161

162 **2.1.2 Temperature, potential evaporation and ET**

163 We obtained the monthly gridded temperature dataset (0.5 degree) from CMA; and
164 potential evaporation (PET) dataset (0.5 degree, Harris et al., 2013) from Climatic
165 Research Unit (CRU), University of East Anglia. Moreover, we used six global
166 /regional ET products (four diagnostic products and two LSMs simulations, Table 2),
167 namely (1) GLEAM_E (Miralles et al., 2010, 2011), which consists of three sources
168 of ET (transpiration, soil evaporation and interception) for bare soil, short vegetation
169 and vegetation with a tall canopy calculated using a set of algorithm (www.gleam.eu),



170 (2) GNoah_E simulated using GLDAS-2 with the Catchment Noah scheme
171 (<http://disc.sci.gsfc.nasa.gov/hydrology/data-holdings>) (Rodell et al., 2004), (3)
172 Zhang_E (Zhang et al., 2010), which is estimated using the modified
173 Penman-Monteith equation forced with MODIS data, satellite-based vegetation
174 parameters and meteorological observations (<http://www.ntsug.umd.edu/project/et/>), (4)
175 MET_E (Jung et al., 2010) (<https://www.bgc-jena.mpg.de/geodb/projects/Home.phs>),
176 (5) VIC_E (Zhang et al., 2014) from VIC_IGSNRR simulations
177 (http://hydro.igsnrr.ac.cn/public/vic_outputs.html) and (6) PML_E (Zhang Y. et al.,
178 2016) computed from global observation-driven Penman-Monteith-Leuning (PML)
179 model (<https://data.csiro.au/dap/landingpage?pid=csiro:17375&v=2&d=true>).
180

181 **2.1.3 Vegetation and snow/glacier parameters**

182 To quantify the dynamics of vegetation of each river basin, we applied the
183 Normalized Difference Vegetation Index (NDVI) and the Leaf Area Index (LAI)
184 (Table 1). Briefly, the NDVI data was obtained from the Global Inventory Modeling
185 and Mapping Studies (GIMMS) (Turker et al., 2005)
186 (https://nex.nasa.gov/nex/projects/1349/wiki/general_data_description_and_access/)
187 while the LAI data was collected from the Global Land Surface Satellite (GLASS)
188 products (<http://www.glcg.umd.edu/data/lai/>) (Liang and Xiao, 2012). Whist the
189 change in seasonal snow cover and glacier has significant impact on the water and
190 energy budgets in TP river basins; it remains a technical challenge to get reliable
191 observations due to harsh environment (especially at the basin scale). However,
192 recently available satellite-based/LSM-simulated products might provide adequate
193 characterization of the variation of snow cover and glacier. To quantify the change in



194 snow cover at each basin, we applied the daily cloud free snow composite product
195 from MODIS Terra-Aqua and the Interactive Multisensor Snow and Ice Mapping
196 System for the Tibetan Plateau (Zhang et al., 2012; Yu et al., 2015), in conjunction
197 with the snow water equivalent (SWE) retrieved from Global Snow Monitoring for
198 Climate Research product (GlobSnow-2, <http://www.globsnow.info/>) and the
199 VIC_IGSNRR simulations (Takala et al., 2011; Zhang et al., 2014). We extracted
200 general distribution of glacier of TP from the Second Glacier Inventory Dataset of
201 China (Guo et al., 2014). All gridded datasets used were first uniformly interpolated to
202 a spatial resolution of 0.5 degree based on the bilinear interpolation to make their
203 inter-comparison possible. The datasets were then extracted for each of TP basins.

204

205 **2.1.4 Monsoon indices**

206 In general, the TP climate is under the influences of the westerlies, Indian summer
207 monsoon and East Asian summer monsoon (Yao et al., 2012). To investigate the
208 changes of monsoon systems and their potential impacts on water budgets in the TP
209 basins, we used three monsoon indices, namely Asian Zonal Circulation Index (AZCI),
210 Indian Ocean Dipole Mode Index (IODMI) and East Asian Summer Monsoon Index
211 (EASMI). Briefly, the IODMI (reflects the dynamics of Indian Summer Monsoon) is
212 an indicator of the east-west temperature gradient across the tropical Indian Ocean
213 (Saji et al., 1999), which can be downloaded from the following website:
214 [http://www.jamstec.go.jp/frcgc/research/d1/iod/HTML/Dipole%20Mode%20Index.ht](http://www.jamstec.go.jp/frcgc/research/d1/iod/HTML/Dipole%20Mode%20Index.html)
215 [ml](http://www.jamstec.go.jp/frcgc/research/d1/iod/HTML/Dipole%20Mode%20Index.html). The EASMI and AZCI (60°-150°E) reflect the dynamics of East Asian summer
216 monsoon (Li and Zeng, 2002) and the westerlies (represented by Asian Zonal
217 Circulation index), which can be obtained from Beijing Normal University
218 (<http://ljp.gcess.cn/dct/page/65577>) and the National Climate Center of China



(<http://ncc.cma.gov.cn/Website/index.php?ChannelID=43WCHID=5>), respectively.

220

2.1.5 Study basins

In this study, we selected 18 river basins of varied sizes (range: 2832-191235 km²; see Table 1 for details) with adequate runoff data over a 30-year period (1982-2011). They are distributed in the northwestern, southeastern and eastern parts of the plateau with multiyear-mean and basin-averaged temperature and precipitation ranging from -5.68 to 0.97 °C and 128 to 717 mm, which are solely dominated or under the combined influences of the westerlies, the Indian Summer monsoon and the East Asian monsoon (Yao et al., 2012). There are more glacier and snow covers in the westerlies-dominant basins such as Yerqiang, Yulongkashi and Keliya (10.86~23.27% and 29.16~35.95%, respectively); less for the East Asian monsoon-dominated basins such as Yellow, Yangtze and Bayin (0~0.96% and 9.42~20.05%, respectively) (Table 2).

233

234

235

2.2 Methods

2.2.1 Water balance-based ET estimation

The basin-wide water balance at the monthly and annual timescales could be written as the principle of mass conservation (also known as the continuity equation, Oliveira et al., 2014) of basin-wide precipitation (P, mm), evapotranspiration (ET_{wb}, mm), runoff (Q, mm) as well as terrestrial water storage change (ΔS, mm),

$$ET_{wb} = P - Q - \Delta S \quad (1)$$

The terrestrial water storage (ΔS) in Eq. (1) includes the surface, subsurface and



ground water changes. It has been demonstrated cannot be neglected in water balance calculation over monthly and annual timescales due to snow cover change and anthropogenic interferences (e.g., reservoir operation, agricultural water withdrawal) (Liu et al., 2016a). For the period 2002-2011, we calculated basin-wide ET (ET_{wb}) directly using the GRACE-derived ΔS in Eq. (1). Since GRACE data is absent before 2002, we calculated the monthly ET_{wb} using the following two-step bias-correction procedure (Li X. et al., 2014). We defined $P - Q$ in Eq. (1) as biased ET (ET_{biased} , available from 1982 to 2011) relative to the “true” ET ($ET_{wb} = P - Q - \Delta S$, available during the period 2002-2011 when the GRACE data is available). Over the period 2002-2011, we first fitted ET_{biased} and ET_{wb} series separately using different gamma distributions, which has been evidenced as an proper method for modeling the probability distribution of ET (Bouraoui et al., 1999). The monthly ET_{biased} series (2002-2011) can then be bias-corrected through the inverse function (F^{-1}) of the gamma cumulative distribution function (CDF, F) of ET_{wb} by matching the cumulative probabilities between two CDFs as follow (Liu et al., 2016a),

$$ET_{corrected}(m) = F^{-1}(F(ET_{biased}(m)|\alpha_{biased}, \beta_{biased})|\alpha_{wb}, \beta_{wb}) \quad (2)$$

Here $\alpha_{biased}, \beta_{biased}$ and α_{wb}, β_{wb} are shape and scale parameters of gamma distributions for ET_{biased} and ET_{wb} . $ET_{corrected}(m)$ and $ET_{biased}(m)$ represent the monthly corrected and biased ET, respectively. The bias correction procedure can be flexibly applied to the period 1983-2011 by matching the CDF of ET_{biased} (1983-2011) to that of $ET_{corrected}$ (2002-2011). The second step of bias correction is to eliminate the annual bias through the ratio of annual ET_{biased} to annual $ET_{corrected}$ calculated in the first step using the following method,



$$ET_{\text{final}}(m) = \frac{ET_{\text{biased}}(a)}{ET_{\text{corrected}}(a)} \times ET_{\text{corrected}}(m) \quad (3)$$

where $ET_{\text{final}}(m)$ is the final monthly ET after bias correction. $ET_{\text{biased}}(a)$ and $ET_{\text{corrected}}(a)$ represent the annual biased and corrected ET while $ET_{\text{corrected}}(m)$ is the monthly corrected ET obtained from the first step. The procedure was then applied to correct the monthly ET_{biased} series and calculated the monthly $ET_{\text{corrected}}$ during the period 1982-2001 for all TP basins. We take these results as sufficient representation of the “true” ET (ET_{wb}) for evaluating multiple ET products and trend analysis. ”

2.2.2 Modified Mann-Kendall test method

The Mann-Kendall (MK) test is a rank-based nonparametric approach which is less sensitive to outlier relative to other parametric statistics, but it is sometimes influenced by the serial correlation of time series. Pre-whitening is often used to eliminate the influence of lag-1 autocorrelation before the use of MK test. For example, $X(X_1, X_2, \dots, X_n)$ is a time series data, it will be replaced by $(X_2 - cX_1, X_3 - cX_2, \dots, X_{n+1} - cX_n)$ in pre-whitening if the lag-1 autocorrelation coefficient (c) is larger than 0.1 (von Storch, 1995). However, significant lag-1 autocorrelation may still be detected after pre-whitening because only the lag-1 autocorrelation is considered in pre-whitening (Zhang et al., 2013). Moreover, it sometimes underestimate the trend for a given time series (Yue et al., 2002). Hamed and Rao (1998) proposed a modified version of MK test (MMK) to consider the lag-1 autocorrelation and related robustness of the autocorrelation through the use of equivalent sample size, which has been widely used in previous studies during the last five decades (McVicar et al., 2012; Zhang et al., 2013; Liu and Sun, 2016). In the MMK approach, if the lag-1 autocorrelation coefficients are significantly distinct from



293 zero, the original variance of MK statistics will be replaced by the modified one. In
294 this study, we used the MMK approach to quantify the trends of water budget
295 components in 18 TP basins and the significance of trend was tested at the >95%
296 confidence level.

297

298 **2.2.3 Uncertainty analysis**

299 The uncertainty associated multi-source dataset used (no observation or the
300 observations are not adequate at the basin scale) for quantifying the dynamics of
301 certain water budget components (i.e., ET and precipitation) are also analyzed. We
302 investigate the seasonal cycles and trends of these components by using different
303 datasets together in the analysis to show the potential uncertainties in this study.

304

305 **3 Results and Discussion**

306 **3.1 ET evaluation and General hydrological characteristics of 18 TP basins**

307 We first assessed the VIC_IGSNRR simulated runoff against the observations for
308 each basin (for example, at Tangnaihai and Pangduo stations in Fig.2). If the Nash
309 Efficiency coefficient (NSE) between the observation and simulation is above 0.65,
310 the VIC_IGSNRR simulated runoff is acceptable and could be used to replace the
311 missing runoff values for a given basin. Moreover, the CMA precipitation is
312 consistent with TRMM (Corr = 0.86, RMSE = 8.34 mm/month) and IGSNRR forcing
313 (Corr = 0.94, RMSE = 7.15mm/month) precipitation for multiple basins (i.e., for the
314 smallest basin above Tongren station, Fig.2). Moreover, the magnitudes of
315 GRACE-derived annual mean water storage change (ΔS) in 18 TP basins are
316 relatively less than those for other water balance components such as annual P, Q and
317 ET (Table 3). The uncertainties among GRACE-derived annual mean ΔS from



different data processing centers (CSR, GFZ and JPL) are small for 18 basins except for the basins controlled by Gadatan and Tangnaihahai stations.

We then evaluated six ET products in 18 TP basins against our calculated ET_{wb} at a monthly basis during the period 1983-2006 (Fig. 3). The ranges of monthly averaged ET among different basins (approximately 4–39 mm month⁻¹) are very close for all products compare to that calculated from the ET_{wb} (6–42 mm month⁻¹). However, GLEAM_E (correlation coefficient: Corr = 0.85 and root-mean-square-error: RMSE = 5.69 mm month⁻¹) and VIC_E (Corr = 0.82 and RMSE = 6.16 mm month⁻¹) perform relatively better than others. Although Zhang_E and GNoah_E were found closely correlated to monthly ET_{wb} in the upper Yellow River, the upper Yangtze River, Qiangtang and Qaidam basins (Li X. et al., 2014), they did not exhibit overall good performances (Corr = 0.61, RMSE = 7.97 mm month⁻¹ for Zhang_E and Corr = 0.42, RMSE = 10.16 mm month⁻¹ for GNoah_E) for 18 TP basin used in this study. We thus use GLEAM_E and VIC_E together with ET_{wb} to analyze the seasonal cycles and trends of ET in 18 TP basins in the following sections.

To investigate the general hydroclimatic characteristics of river basins over the TP, we classify 18 basins into three categories, namely westerlies-dominated basins (Yerqiang, Yulongkashi and Kelia), Indian monsoon-dominated basins (Brahmaputra and Salween), and East Asian monsoon-dominated basins (Yellow, Yalong and Yangtze) referred to Tian et al. (2007), Yao et al. (2012) and Dong et al. (2016). Interestingly, they are clustered into three groups under Budyko framework (Budyko, 1974; Zhang D. et al., 2016) with relatively lower evaporative index in Indian



monsoon-dominant basins and higher aridity index in westerlies-dominant basins, which reveal various long-term hydroclimatologic conditions (Fig. 4). Overall, the annual mean air temperature increases ($-5.68 \sim 0.97$ °C) while multiyear mean glacier area (and thus the glacier melt normalized by precipitation) decreases ($23.27 \sim 0\%$) gradually from the westerlies-dominant, Indian monsoon-dominant to East Asian monsoon-dominant basins. The vegetation status (NDVI range: $0.05 \sim 0.43$; LAI range: $0.03 \sim 0.83$) tends to be better and ET increases (and thus runoff coefficient gradually decreases) from cold to warm basins (Fig. 4 and Table 1). The R^2 between basin-averaged NDVI and ET is 0.76 which shows a clear vegetation control on ET in 18 TP basins. The results are in line with Shen et al. (2015), which indicated that the spatial pattern of ET trend was significantly and positively correlated with NDVI trend over the TP. The dominant climate systems are overall discrepant for the three TP regions with different water-energy characteristics and sources of water vapor. The westerlies-controlled basins are relatively colder than the Indian monsoon-dominated basins, thus they develop more glaciers (and thus have more snow melt contributions to total river streamflow) and have relatively less vegetation (and thus limit vegetation transpiration). It is a general picture of hydrological regime in high-altitude and cold regions (Zhang et al., 2013; Cuo et al., 2014), which could be interpreted from the perspective of multi-source datasets in the data-sparse TP.

362

3.2 Seasonal cycles of basin-wide water budget components for the TP basins

The multi-year means of water budget components (i.e., P, Q, ET, snow cover and SWE) and vegetation parameters (i.e., NDVI and LAI) are calculated for each calendar month and for 18 TP river basins using multi-source datasets available from 1982 to 2011. Overall, the seasonal variations of P, Q, ET, air temperature and



368 vegetation parameters are similar in all TP basins with peak values occurred in May to
369 September (Fig.5 and Fig.6). The seasonal cycles of snow cover and SWE are
370 generally consistent among the basins (the peak values mainly occur from October to
371 next April, Fig.7). With the ascending air temperature from cold to warm months, the
372 basin-wide precipitation increases and vegetation cover expands gradually (the
373 basin-wide ET also increase). Meanwhile, snow cover and glaciers retreat gradually
374 with the melt water supplying the river discharge together with precipitation. The
375 inter-basin variations of hydrological regime are to a large extent linked to the climate
376 systems that prevail over the TP.

377

378 Although the temporal patterns of hydrological components are generally analogous,
379 they vary among the parameters, climate zones and even basins (Zhou et al., 2005).
380 For example, relative to air temperature, the seasonal pattern of runoff is similar to
381 precipitation which reveals that runoff is mainly controlled by precipitation in most
382 TP basins. It is in agreement with that summarized by Cuo et al. (2014). In the
383 westerlies-dominated basins, the peak values of precipitation and runoff mainly
384 concentrate in June-August, which contribute approximately 68-82% and 67-78% of
385 annual totals, respectively. During this period, the runoff always exceeds precipitation
386 which indicates large contributions of glacier/snow-melt water to streamflow. It is
387 consistent with the existing findings in Tarim River (Yerqiang, Yulongkashi and
388 Keliya rivers are the major tributaries of Tarim River), which indicated that the melt
389 water accounted for about half of the annual total streamflow (Fu et al., 2008). The
390 ET (vegetation cover) in three westerlies-dominated basins are relatively less (scarcer)
391 than that in other TP basins while the percentages of glacier and seasonal snow cover
392 are higher in these basins which contribute more melt water to river discharge (Fig.6



393 and Fig.7). Overall, the SWE in Yerqiang, Yulongkashi and Keliya rivers are higher in
394 winter than other seasons, but they vary with basins and products which reflect
395 considerable uncertainties in SWE estimations.

396

397 In the Indian monsoon and East Asian monsoon dominated basins, the runoff
398 concentrates during June-September (or June- October) with precipitation being the
399 dominant contributor of annual total runoff. For example, the peak values of
400 precipitation and runoff occur during June-September at Zhimenda station
401 (contributing about 80% and 74% of the annual totals) while those occur during
402 June-October at Tangnaihai station (contributing about 78% and 71% of the annual
403 totals, respectively). The results are quite similar to the related studies in eastern and
404 southern TP such as Liu (1999), Dong et al. (2007), Zhu et al. (2011), Zhang et al.
405 (2013), Cuo et al. (2014). The vegetation cover (ET) in most basins is denser (higher)
406 than that in the westerlies-dominant basins. Moreover, the seasonal snow mainly
407 covers from mid-autumn to spring and correspondingly the SWE is relatively higher
408 in these months in all basins except for Yellow River above Xining station, Salwee
409 River above Jiayuqiao station and Brahmaputra River above Nuxia and Yangcun
410 stations.

411

412 3.3 Trends of basin-wide water budget components for the TP basins

413 The Q , P and ET_{wb} all ascended under regional warming during the past 30 years in
414 the westerlies-dominated basins (Fig.8), except for P in the Yerqiang River basin
415 (Kulukelangan station). The aridity index (PET/P), which is an indicator for the
416 degree of dryness, slightly declined in all basins in northwestern TP. Although both P
417 and PET were found increase in the Keliya River basin since the 1980s (Shi et al.,



2003; Yao et al., 2014), the declined PET/P is, to some extent, attributed to the ascending P exceed the increase in PET. The climate moistening (Shi et al., 2003) in the headwaters of these inland rivers would be beneficial to the water resources and oasis agro-ecosystems in the middle and lower basins. The increase in streamflow was also found in most tributaries of the Tarim River (Sun et al., 2006; Fu et al., 2010; Mamat et al., 2010). Moreover, the westerlies, revealed by the Asian Zonal Circulation Index (60°-150° E), slightly enhanced (linear trend: 0.21) over the period 1982-2011 (Fig.9). With the strengthening westerlies, more water vapor may be transported and fell as precipitation or snow in northwestern TP (e.g., the eastern Pamir region). Both SWE products (VIC_IGSNRR simulated and GlobaSnow-2 product) showed slightly increase across these basins with rising seasonal snow covers and glaciers (Yao et al., 2012). More precipitation was transformed into snow /glacier and the runoff coefficient (Q/P) exhibited decrease with precipitation obviously increased (Fig.8). In addition, the transpiration in these basins might decrease with vegetation degradation as revealed by the NDVI and LAI (Yin et al., 2016) but the atmospheric evaporative demand indicated by CRU PET increased (significantly increase in the Yulongkashi and Keliya rivers) during the period 1982-2011.

436

437

In the East Asian monsoon dominated basins, there are two types of change for basin-wide water budget components. For example, P and Q slightly decreased in the upper Yellow River (Tangnihai, Huangheyan and Jimai stations) and Yalong River (Yajiang station) but increased in other basins (Zelingou, Gandatan, Xining, Tongren and Zhimenda stations) over the period of 1982-2011 (Fig.10). The declined Q and P in



the upper Yellow and Yalong Rivers (located at the eastern Tibetan Plateau) were consistent with that found by Cuo et al. (2013, 2014) and Yang et al. (2014), and were in line with the weakening East Asian Summer Monsoon (linear slope: -0.01) (Fig.9). The vegetation turned green while ET_{wb} and PET increased in all East Asian monsoon dominated basins (except for ET_{wb} in the basins above Tongren and Yajing stations) with the significantly ascending air temperature during the period 1982-2011. The aridity index (PET/P) decreased in all basins except for the upper Yellow River basin above Jimai station and the upper Yalong River basin above Yajiang station. Moreover, both the runoff coefficients and SWE decreased except for the Bayin River above Zelingou station and the upper Yellow River above Tongren station in the East Asian monsoon dominated basins.

The P, ET_{wb} and Q also increased in the Indian monsoon-dominated basins (except for ET_{wb} in the basin above Yangcun station) such as Salween River and Brahmaputra River (Fig.11), which are in line with the strengthening (linear trend: 0.01) of the Indian summer monsoon (revealed by the Indian Ocean Dipole Mode Index) during the specific period 1982-2011 (Fig.9). For example, at Jiayuqiao station, the annual streamflow showed a slightly increasing trend which was consistent with that examined by Yao et al. (2012) during the period 1980-2000. The vegetation status, revealed by NDVI and LAI, turned better associated with the ascending air temperature. The aridity index (PET/P) decreased in all basins except for the Brahmaputra River above Tangjia station, which indicated that most basins in the Indian monsoon-dominated regions turned wet over the period of 1982-2011. The runoff coefficient (Q/P) increased at Gongbujiangda and Nuxia while decreased at Jiayuqiao, Pangduo, Tangji and Yangcun stations. Moreover, the basin-wide SWE



declined in the upper Salween River and Brahmaputra River above Pangduo, Tangjia
and Gongbujiangda stations while increased in Brahmaputra River above Nuxia and
Yangcun stations.

471

3.4 Uncertainties

The results may unavoidably associate with some uncertainties inherited from the
multi-source datasets used. The primary sources of uncertainty may arise from the
precipitation inputs. We compared the seasonal cycles and annual trends in different
precipitation products, i.e. CMA_P, IGSNRR_P and TRMM_P (and their
calculated ET_{wb} from the water balance) during the period 2000-2011 (Fig. 12 and
Fig. 13). We found there are some uncertainties among different precipitation
products and thus among their estimated ET_{wb} , especially in the westerlies-dominated
basins. However, for each basin, the seasonal cycles of precipitation (and their
calculated ET_{wb}) calculated from different products are overall similar (especially for
the observation-based products, CMA_P and IGSNRR_P). The signs of trend for
annual CMA_P and IGSNRR_P (and their calculated ET_{wb}) are consistent in most
river basins (i.e., 14 out 18 basins for two precipitation products and 17 out 18 basins
for their calculated ET_{wb}) during the period 1982-2011. The consistency of trends
between two precipitation products, to some extent, revealed that the trends in
CMA_P were not obviously influenced by the changing density of rain gauges in TP
basins. Although some uncertainties exist due to limited and unevenly distributed
meteorological stations used in the plateau and the influences of complex terrain,
CMA_P is still the best observation-based precipitation product nowadays in China
which could be applied to hydrological studies in the TP.

492



493

494 Although the seasonal cycles of ET_{wb} could be captured by GLEAM_E and VIC_E,
495 they still have considerable uncertainties at some stations (e.g., Numaitilangan,
496 Gongbujiangda and Nuxia) (Fig.5). Compared to the annual trend of ET_{wb} (Table 4),
497 most ET products (including the well-performed GLEAM_E and VIC_E) could not
498 detect the decreasing trends in 7 out of 18 basins (Kulukelangan, Tongguziluoke,
499 Xining, Tongren, Jimai, Nuxia and Gongbujiangda) due to their different forcing data,
500 algorithm used as well as varied spatial-temporal resolutions (Xue et al., 2013; Li et
501 al., 2014; Liu et al., 2016a). In particular, it is well known that land surface models
502 have some difficulties (e.g., parameter tuning in boundary layer schemes) when
503 applying to the TP, even though they sometimes have good performances in different
504 regions/basins (Xia et al., 2012; Bai et al., 2016). For example, Xue et al. (2013)
505 indicated that GNoah_E underestimated the ET_{wb} in the upper Yellow River and
506 Yangtze River basins on the Tibetan Plateau mainly due to its negative-biased
507 precipitation forcing. We thus only used ET_{wb} in the trend detection of water budget
508 components in Fig.8, Fig.10 and Fig.11 in this study. The two SWE products also
509 showed large uncertainty with respect to both their seasonal cycles and trends. The
510 VIC_IGSNRR simulated and GlobaSnow-2 SWEs have not been validated in the TP
511 due to the lack of snow water equivalent observations, but in some basins (e.g.,
512 Zelingou and Numaitilangan) they showed similar seasonal cycles and annual trends.

513

514 The interpolation of missing values of runoff with VIC_IGSNRR simulated runoff
515 and the gridded precipitation data (which interpolated from limited gauged
516 precipitation over the plateau) also introduced uncertainties. There are also
517 considerable uncertainties arising from empirical extending the ET series back prior



518 to the GRACE era. However, the trends in ET_{wb} have not significantly affected by
519 erroneous trends in the precipitation inputs to the bias-correction based water balance
520 calculation. For example, the trends in CMA_P and IGSNRR_P are opposite in few
521 basins (No. 01, 07, 08, 13 in Fig. 13), but the trends in their calculated ET_{wb} are both
522 consistent for each basin. It is, to some extent, certified the effectiveness of the bias
523 correction-based ET-estimate approach. With these caveats, we can interpret the
524 general hydrological regimes and their responses to the changing climate in the TP
525 basins from solely the perspective of multi-source datasets, which are comparable to
526 the existing studies based on the in situ observations and complex hydrological
527 modeling.

528

529 4 Summary

530 In this study, we investigated the seasonal cycles and trends of water budget
531 components in 18 TP basins during the period 1982-2011, which is not well
532 understood so far due to the lack of adequate observations in the harsh environment,
533 through integrating the multi-source global/regional datasets such as gauge data,
534 satellite remote sensing and land surface model simulations. By using a two-step bias
535 correction procedure, we calculated the annual basin-wide ET_{wb} through the water
536 balance approach considering the impacts of glacier and water storage change. We
537 found that the GLEAM_E and VIC_E perform better relative to other products against
538 the calculated ET_{wb} .

539

540 From the Budyko framework perspective, the general water and energy budgets are
541 different in the westerlies-dominated (with higher aridity index, runoff coefficient and
542 glacier cover), the Indian monsoon-dominated and the East Asian



monsoon-dominated (with higher air temperature, vegetation cover and evapotranspiration) basins. In the 18 TP basins, precipitation is the major contributor to the river runoff, which concentrates mainly during June-October (June-August for the westerlies-dominated basins, June-September or June to October for the Indian monsoon-dominated and the East Asian monsoon-dominated basins). The basin-wide SWE is relatively high from mid-autumn to spring for all 18 TP basins except for Keliya River and Brahmaputra River above the Nuxia and Yangcun stations. The vegetation cover is relatively less whereas snow/glacier cover is more in the westerlies-dominant basins compared to other basins. During the period 1982-2011, we found that the P , Q and ET_{wb} increased across most of the basins in Tibetan Plateau; receded at some tributaries located at the upper Yellow River and Yalong River due to the weakening East Asian monsoon. The aridity index (PET/P) exhibited decrease in most TP basins which corresponded to the warming and moistening climate in the TP and western China. Moreover, the runoff coefficient (Q/P) declined in most basins which may be, to some extent, due to ET increase induced by vegetation greening and the influences of snow and glacier changes. Although there are considerable uncertainties inherited from multi-source data used, the general hydrological regimes in the TP basins could be revealed, which are consistent to the existing results obtained from in situ observations and complex land surface modeling. It indicated the usefulness of integrating the multiple datasets (e.g., in situ observations, remote sensing-based products, reanalysis outputs, land surface model simulations and climate model outputs) for hydrological applications. The generalization here could be helpful for understanding the hydrological cycle and supporting sustainable water resources management and eco-environment protection in the Tibetan Plateau under global warming.



568

569 **Author contributions.** Wenbin Liu and Fubao Sun developed the idea to see the
570 general water budgets in the TP basins from the perspective of multisource datasets.
571 Wenbin Liu collected and processed the multiple datasets with the help of Yanzhong
572 Li, Guoqing Zhang, Wee Ho Lim, Hong Wang as well as Peng Bai, and prepared the
573 manuscript. The results were extensively commented and discussed by Fubao Sun,
574 Jiahong Liu and Yan-Fang Sang.

575

576 **Acknowledgements.** This study was supported by the National Key Research and
577 Development Program of China (2016YFC0401401 and 2016YFA0602402), National
578 Natural Science Foundation of China (41401037 and 41330529), the Open Research
579 Fund of State Key Laboratory of Desert and Oasis Ecology in Xinjiang Institute of
580 Ecology and Geography, Chinese Academy of Sciences (CAS), the CAS Pioneer
581 Hundred Talents Program (Fubao Sun), the CAS President's International Fellowship
582 Initiative (2017PC0068) and the program for the "Bingwei" Excellent Talents from
583 the Institute of Geographic Sciences and Natural Resources Research, CAS. We are
584 grateful to the NASA MEaSUREs Program (Sean Swenson) for providing the
585 GRACE land data processing algorithm. The basin-wide water budget series in the TP
586 Rivers used in this study are available from the authors upon request
587 (liuwb@igsnr.ac.cn). We thank the editors and reviewers for their invaluable
588 comments and constructive suggestions.

589

590 References

591 Akhtar, M., Ahmad, N., and Booij, M.J.: Use of regional climate model simulations as input for
592 hydrological models for the Hindukush-Karakorum-Himalaya region, Hydrol. Earth Syst. Sci.
593 13, 1075-1089, 2009.



- 594 Bai, P., Liu, X.M., Yang, T.T., Liang, K., and Liu, C.M.: Evaluation of streamflow simulation
595 results of land surface models in GLDAS on the Tibetan Plateau, J. Geophys. Res. Atmos., 121,
596 12180-12197, 2016.
- 597 Berrisford, P, Lee, D., Poli, P., Brugge, R., Fielding, K., Fuentes, M., Kallberg, P., Kobayashi, S.,
598 Uppala, S., and Simmons, A.: The ERA-interim archive. ERA Reports Series No. 1 Version 2.0,
599 Available from: <[https://www.researchgate.net/publication/41571692_The_ERA-interim](https://www.researchgate.net/publication/41571692_The_ERA-interim_archive)
600 archive>, 2011.
- 601 Bookhagen, B. and Burbank, D.W.: Toward a complete Himalayan hydrological budget:
602 spatiotemporal distribution of snowmelt and rainfall and their impact on river discharge, J.
603 Geophys. Res., 115, F03019, 2010.
- 604 Bouraoui, F., Vachaud, G., Li, L.Z.X., LeTreut, H., and Chen, T.: Evaluation of the impact of
605 climate changes on water storage and groundwater recharge at the watershed scale, Clim. Dyn.,
606 15(2), 153-161, 1999.
- 607 Budyko, M.I.: Climate and life. Academic Press, 1974.
- 608 Chen, D., Xu, B., Yao, T., Guo, Z., Cui, P., Chen, F., Zhang, R., Zhang, X., Zhang, Y., Fan, J., Hou,
609 Z., and Zhang, T.: Assessment of past, present and future environmental changes on the Tibetan
610 Plateau, Chinese SCI. Bull., 60(32), 3025-3035, 2015 (in Chinese).
- 611 Cuo, L., Zhang, Y.X., Bohn, T.J., Zhao, L., Li, J.L., Liu, Q.M., and Zhou, B.R.: Frozen soil
612 degradation and its effects on surface hydrology in the northern Tibetan Plateau, J. Geophys.
613 Res. Atmos., 120(6), 8276-8298, 2015.
- 614 Cuo, L., Zhang, Y.X., Gao, Y., Hao, Z., and Cairang, L.: The impacts of climate change and land
615 cover/use transition on the hydrology in the upper Yellow River Basin, China, J. Hydrol., 502,
616 37-52, 2013.
- 617 Cuo, L., Zhang, Y.X., Zhu, F.X., and Liang, L.Q.: Characteristics and changes of streamflow on
618 the Tibetan Plateau: A review, J. Hydrol. Reg. stud., 2, 49-68, 2014.
- 619 Dong, X., Yao, Z., and Chen, C.: Runoff variation and responses to precipitation in the source
620 regions of the Yellow River, Resour. Sci., 29(3), 67-73, 2007 (in Chinese).
- 621 Dong, W., Lin, Y., Wright, J.S., Ming, Y., Xie, Y., Wang, B., Luo, Y., Huang, W., Huang, J., Wang,
622 L., Tian, L., Peng, Y., and Xu, F.: Summer rainfall over the southwestern Tibetan Plateau
623 controlled by deep convection over the Indian Subcontinent, Nat. Commun., 7, 10925, 2016.



- 624 Duan, A.M. and Wu, G.X.: Change of cloud amount and the climate warming on the Tibetan
625 Plateau, *Geophys. Res. Lett.*, 33, L22704, 2006.
- 626 Fu, L., Chen, Y., Li, W., Xu, C., and He, B.: Influence of climate change on runoff and water
627 resources in the headwaters of the Tarim River, *Arid Land Geogr.*, 31(2), 237-242, 2008 (in
628 Chinese).
- 629 Fu, L., Chen, Y., Li, W., He, B., and Xu, C.: Relation between climate change and runoff volume
630 in the headwaters of the Tarim River during the last 50 years., *J. Desert Res.*, 30(1), 204-209,
631 2010 (in Chinese).
- 632 Guo, W.Q., Liu, S.Y., Yao, X.J., Xu, J.L., Shangguan, D.H., Wu, L.Z., Zhao, J.D., Liu, Q., Jiang,
633 Z.L., Wei, J.F., Bao, E.J., Yu, P.C., Ding, L.F., Li, G., Ge, C.M., and Wang, Y.: The Second
634 Glacier Inventory Dataset of China, Cold and Arid Regions Science Data Center at Lanzhou,
635 doi: 10.3972/glacier.001.2013.db, 2014.
- 636 Hamed, K.H. and Rao, A.R.: A modified Mann-Kendall trend test for autocorrelation data,
637 *J. Hydrol.*, 204(1-4), 182-196, 1998.
- 638 Huffman, G.J., , E.F., Bolvin, D.T., Nelkin, E.J., and Adler, R.F.: last updated 2013: TRMM
639 Version 7 3B42 and 3B43 Data Sets, NASA/GSFC, Greenbelt, MD. Data set accessed at
640 [http://mirador.gsfc.nasa.gov/cgi-bin/mirador/](http://mirador.gsfc.nasa.gov/cgi-bin/mirador/presentNavigation.pl?tree=project&project=TRMM&dataGroup=Gridded&CGIS)
641 [presentNavigation.pl?tree=project&project=TRMM&dataGroup=Gridded&CGIS](http://mirador.gsfc.nasa.gov/cgi-bin/mirador/presentNavigation.pl?tree=project&project=TRMM&dataGroup=Gridded&CGIS)
642 [ESSID=5d12e2ffa38ca2aac6262202a79d882a](http://mirador.gsfc.nasa.gov/cgi-bin/mirador/presentNavigation.pl?tree=project&project=TRMM&dataGroup=Gridded&CGIS), 2012.
- 643 Harris, I., Jones, P.D., Osborn, T.J., and Lister, D.H.: Updated high-resolution grids of monthly
644 climatic observations – the CRU TS3.10 Dataset, *Int. J. Climatol.*, 34 (3), 623-642, 2014.
- 645 Immerzeel, W.W., van Beek, L.P.H., and Bierkens, M.F.P.: Climate change will affect the Asian
646 water towers, *Science*, 328, 1382-1385, 2010.
- 647 Jung, M., Reichstein, M., Ciais, P., Seneviratne, S.I., Sheffield, J., Goulden, M.L., Bonan, G.,
648 Cescatti, A., Chen, J., de Jeu, R., Dolman, A.J., Eugster, W., Gerten, D., Gianelle, D., Gobron, N.,
649 Heinke, J., Kimball, J., Law, B.E., Montagnani, L., Mu, Q., Mueller, B., Oleson, K., Papale, D.,
650 Richardson, A.D., Rouspard, O., Running, S., Tomelleri, E., Viovy, N., Weber, U., Williams, C.,
651 Wood, E., Zaehle, S., and Zhang, K.: Recent decline in the global land evapotranspiration trend



- 652 due to limited moisture supply, *Nature*, 467, 951-954, 2010.
- 653 Kobayashi, S., Ota, Y., Harada, Y., Ebata, A., Moriya, M., Onoda, H., Onogi, K., kamahori, H.,
- 654 kobayashi, C., Endo, H., miyaoka, K., and Takahashi, K.: The JRA-55 Reanalysis: General
- 655 specifications and basic characteristics, *J.Meteor. Soc. Japan*, 93(1), 5-58, doi:
- 656 10.2151/jmsj.2015-001, 2015.
- 657 Landerer, F.W. and Swenson, S.C.: Accuracy of scaled GRACE terrestrial water storage estimates,
- 658 *Water Resour.Res.*, 48, W04531, 2012.
- 659 Li, F.P., Zhang, Y.Q., Xu, Z.X., Liu, C.M., Zhou, Y.C., and Liu, W.F.: Runoff predictions in
- 660 ungauged catchments in southeast Tibetan Plateau, *J. Hydrol.*, 511, 28-38, 2014.
- 661 Li, F.P., Zhang, Y.Q., Xu, Z.X., Teng, J., Liu, C.M., Liu, W.F., and Mpelasoka, F.: The impact of
- 662 climate change on runoff in the southeastern Tibetan Plateau, *J. Hydrol.*, 505, 188-201, 2013.
- 663 Li, J.P. and Zeng, Q.C.: A unified monsoon index, *Geophys. Res. Lett.*, 29(8), 1274, 2002.
- 664 Li, X.P., Wang, L., Chen, D.L., Yang, K., and Wang, A.H.: Seasonal evapotranspiration changes
- 665 (1983-2006) of four large basins on the Tibetan Plateau, *J. Geophys. Res.*, 119 (23),
- 666 13079-13095, 2014.
- 667 Liang, S.L. and Xiao, Z.Q.: Global Land Surface Products: Leaf Area Index Product Data
- 668 Collection(1985-2010), Beijing Normal University, doi:10.6050/glass863.3004.db, 2012.
- 669 Liu, T.: Hydrological characteristics of Yalungzangbo River, *Acta Geogr. Sin.*, 54 (Suppl.),
- 670 157-164, 1999 (in Chinese).
- 671 Liu, W.B. and Sun, F.B.: Assessing estimates of evaporative demand in climate models using
- 672 observed pan evaporation over China, *J. Geophys. Res. Atmos.*, 121, 8329-8349, 2016.
- 673 Liu, W.B., Wang, L., Zhou, J., Li, Y.Z., Sun, F.B., Fu, G.B., Li, X.P., and Sang, Y-F.: A worldwide
- 674 evaluation of basin-scale evapotranspiration estimates against the water balance method, *J.*
- 675 *Hydrol.*, 538, 82-95, 2016a.
- 676 Liu, W.B., Wang, L., Chen, D.L., Tu, K., Ruan, C.Q., and Hu, Z.Y.: Large-scale circulation
- 677 classification and its links to observed precipitation in the eastern and central Tibetan Plateau,
- 678 *Clim. Dyn.*, 46, 3481-3497, 2016b.
- 679 Liu, X.M., Yang, T., Hsu, K., Liu, C., and Sorooshian, S.: Evaluating the streamflow simulation



- 680 capability of PERSIANN-CDR daily rainfall products in two river basins on the Tibetan Plateau,
681 Hydrol. Earth Syst. Sci., 21, 169-181, 2017.
- 682 Long, D., shen, Y.J., Sun, A., Hong, Y., Longuevergne, L., Yang, Y.T., Li, B., and Chen, L.:
683 Drought and flood monitoring for a large karst plateau in Southwest China using extended
684 GRACE data, Remote Sen. Environ., 155, 145-160, 2014.
- 685 Lucchesi, R.: File specification for MERRA products, GMAO Office Note No.1 (version 2.3), 82
686 pp, available from http://gmao.gsfc.nasa.gov/pubs/office_notes, 2012.
- 687 Ma, N., Szilagyi, J., Niu, G.Y., Zhang, Y.S., Zhang, T., Wang, B.B., and Wu, Y.H.: Evaporation
688 variability of Nam Co Lake in the Tibetan Plateau and its role in recent rapid lake expansion, J.
689 Hydrol., 537, 27-35, 2016.
- 690 Ma, N., Zhang, Y.S., Guo, Y.H., Gao, H.F., Zhang, H.B., and Wang, Y.F.: Environmental and
691 biophysical controls on the evapotranspiration over the highest alpine steppe, J. Hydrol., 529,
692 980-992, 2015.
- 693 Mamat, A., Halik, W., and Yang, X.: The climatic changes of Qarqan river basin and its impact on
694 the runoff, Xinjiang Agric. Sci., 47 (5), 996-1001, 2010 (in Chinese).
- 695 McVicar, T.R., Roderick, M., Donohue, R.J., Li, L.T., Van Niel, T.G., Thomas, A., Grieser, J.,
696 Jhajharia, D., Himri, Y., Mahowald, N.M., Mescherskaya, A.V., Kruger, A.C., Rehman, S., and
697 Dinpashoh, Y.: Global review and synthesis of trends in observed terrestrial near-surface wind
698 speeds: implications for evaporation, J. Hydrol., 416-417, 182-205, 2012.
- 699 Miralles, D.G., De Jeu, R.A.M., Gash, J.H., Holmes, T.R.H., and Dolman, A.J.: Magnitude and
700 variability of land evaporation and its components at the global scale, Hydrol. Earth Syst. Sci., 15,
701 967-981, 2011.
- 702 Miralles, D.G., Gash, J.H., Holmes, T.R.H., de Jeu, R.A.M, and Dolman, A.J.: Global canopy
703 interception from satellite observations, J. Geophys. Res., 115, D16122, 2010.
- 704 Oliveira, P.T.S., Mearing, M.A., Moran, M.S., Goodrich, D.C., Wendland, E., and Gupta, H.V.:
705 Trends in water balance components across the Brazilian Cerrado, Water Resour. Res., 50,
706 7100-7114, 2014.
- 707 Rodell, M., Houser, P.R., Jambor, U., Gottschalck, J., Mitchell, K., Meng, C.-J., Arsenault, K.,
708 Cosgrove, B., Radakovich, J., Bosilovich, M., Entin, J.K., Walker, P., Lohmann, D., and Toll, D.:
709 The global land data assimilation system, B. Am. Meteorol. Soc., 85, 381-394, 2004.



- 710 Rui, H.: README Document for Global Land Data Assimilation System Version 2 (GLDAS-2)
- 711 Products, GES DISC, 2011.
- 712 Saji, N.H., Goswami, B.N., Vinayachandran, P.N., and Yamagata, T.: A dipole mode in the tropical
- 713 Indian Ocean, *Nature*, 401, 360-363, 1999.
- 714 Shen, M.G., Piao, S.L., Jeong, S., Zhou, L.M., Zeng, Z.Z., Ciais, P., Chen, D.L., Huang, M.T., Jin,
- 715 C.S., Li, L.Z.X., Li, Y., Myneni, R.B., Yang, K., Zhang, G.X., Zhang, Y.J., and Yao, T.D.:
- 716 Evaporative cooling over the Tibetan Plateau induced by vegetation growth, *Proc. Natl. Acad.*
- 717 *Sci. U. S.A.*, 112(30), 9299-9304, 2015.
- 718 Shi, Y.F., Shen, Y.P., Li, D.L., Zhang, G.W., Ding, Y.J., Hu, R.J., and Kang, E.S.: Discussion on
- 719 the present climate change from Warm2dry to Warm2wet in northwest China, *Quat. Sci.*, 23(2),
- 720 152-164, 2003 (in Chinese).
- 721 Shepard, D.S.: Computer mapping: the SYMAP interpolation algorithm. *Spatial Statistics and*
- 722 *Models*, G.L. Gaile and C.J. Willmott, Eds., D. Reidel, 133-145, 1984.
- 723 Sun, B., Mao, W., Feng, Y., Chang, T., Zhang, L., and Zhao, L.: Study on the change of air
- 724 temperature, precipitation and runoff volume in the Yarkant River basin, *Arid Zone Res.*, 23(2),
- 725 203-209, 2006 (in Chinese).
- 726 Takala, M., Luojus, K., Pulliainen, J., Derksen, C., Lemmetyinen, J., Kärnä J.-P., Koskinen, J., and
- 727 Bojkov, B.: Estimating northern hemisphere snow water equivalent for climate research through
- 728 assimilation of spaceborne radiometer data and ground-based measurements, *Remote*
- 729 *Sens. Environ.*, 115 (12), 3517-3529, 2011.
- 730 Tapley, B.D., Bettadpur, S., Watkins, M., and Randerger, C.: The gravity recovery and climate
- 731 experiment: mission overview and early results, *Geophys. Res. Lett.*, 31, L09607, 2004.
- 732 Tian, L., Yao, T., MacClune, K., White, J.W.C., Schilla, A., Vaughn, B., Vachon, R., and
- 733 Ichiyonagi, K.: Stable isotopic variations in west China: a consideration of moisture sources, *J.*
- 734 *Geophys. Res. Atmos.*, 112, D10112, 2007.
- 735 Tucker, C.J., Pinzon, J.E., Brown, M.E., Slayback, D., Pak, E.W., Mahoney, R., Vermote, E., and
- 736 El Saleous, N.: An extended AVHRR 8 km NDVI data set compatible with MODIS and SPOT
- 737 vegetation NDVI data, *Int. J. Remote Sens.*, 26(20), 4485-4498, 2005.



- 738 von Storch, H.: Misuses of statistical analysis in climate research, In Analysis of Climate
- 739 Variability: Applications of Statistical Techniques, Springer-Verlag: Berlin, 11-26, 1995.
- 740 Wang, A. and Zeng, X.: Evaluation of multireanalysis products within site observations over the
- 741 Tibetan Plateau, J. Geophys. Res., 117, D05102, 2012.
- 742 Wang, L., Sun, L.T., Shrestha, M., Li, X.P., Liu, W.B., Zhou, J., Yang, K., Lu, H., and Chen, D.L.:
- 743 Improving snow process modeling with satellite-based estimation of
- 744 near-surface-air-temperature lapse rate, J. Geophys. Res. Atmos., 121, 12005-12030, 2016.
- 745 Xia, Y., Mitchell, K., Ek, M., Cosgrove, B., Sheffield, J., Luo, L., Alonge, C., Wei, H., Meng, J.,
- 746 Livneh, B., and Duang, Q.: Continental-scale water and energy flux analysis and validation for
- 747 North American Land Data Assimilation System project phase 2 (NLDAS-2): 2. Validation of
- 748 model-simulated streamflow, J. Geophys. Res. Atmos., 117(D3), D03110, 2012.
- 749 Xu, L.: The land surface water and energy budgets over the Tibetan Plateau, Available from
- 750 Nature Precedings < <http://hdl.handle.net/10101/npre.2011.5587.1> >, 2011.
- 751 Xue, B.L., Wang, L., Yang, K., Tian, L., Qin, J., Chen, Y., Zhao, L., Ma, Y., Koike, T., Hu, Z., and
- 752 Li, X.P.: Modeling the land surface water and energy cycle of a mesoscale watershed in the
- 753 central Tibetan Plateau with a distributed hydrological model, J. Geophys. Res. Atmos., 118,
- 754 8857-8868, 2013.
- 755 Yao, Z., Duan, R., and Liu, Z.: Changes in precipitation and air temperature and its impacts on
- 756 runoff in the Nujiang River basins. Resour. Sci. 34(2), 202-210, 2012 (in Chinese)
- 757 Yang, K., Qin, J., Zhao, L., Chen, Y.Y., Tang, W.J., Han, M.L., Lazhu, Chen, Z.Q., Lv, N., Ding,
- 758 B.H., Wu, H., and Lin, C.G.: A multi-scale soil moisture and freeze-thaw monitoring network
- 759 on the third pole, Bull. Am. Meteorol. Soc., 94, 1907-1916, 2013.
- 760 Yang, K., Wu, H., Qin, J., Lin, C.G., Tang, W.J., and Chen, Y.Y.: Recent climate changes over the
- 761 Tibetan Plateau and their impacts on energy and water cycle: a review, Glob. Planet Change,
- 762 112, 79-91, 2014.
- 763 Yao, T.D., Thompson, L., Yang, W., Yu, W.S., Gao, Y., Guo, X.J., Yang, X.X., Duan, K.Q., Zhao,
- 764 H.B., Xu, B.Q., Pu, J.C., Lu, A.X., Xiang, Y., Kattel, D.B., and Joswiak, D.: Different glacier
- 765 status with atmospheric circulations in Tibetan Plateau and surroundings, Nat. Clim. Change, 2,
- 766 1-5, 2012.
- 767 Yao, Y.J., Zhao, S.H., Zhang, Y.H., Jia, K., and Liu, M.: Spatial and decadal variations in potential



- 768 evapotranspiration of China based on reanalysis datasets during 1982-2010, *Atmosphere*, 5,
769 737-754, 2014.
- 770 Yin, G., Hu, Z.Y., Chen, X., and Tiyp, T.: Vegetation dynamics and its response to climate change
771 in Central Asia, *J. Arid Land*, 8, 375, 2016.
- 772 Yu, J., Zhang, G., Yao, T., Xie, H., Zhang, H., Ke, C., and Yao, R.: Developing daily cloud-free
773 snow composite products from MODIS Terra-Aqua and IMS for the Tibetan Plateau, *IEEE*
774 *Trans. Geosci. Remote Sens.*, 54(4), 2171-2180, 2015.
- 775 Yue, S., Pilon, P., Phinney, B., Cavadias, G.: The influence of autocorrelation on the ability to
776 detect trend in hydrological series, *Hydrol. Process.*, 16(9), 1807-1829, 2002.
- 777 Zhang, D., Liu, X., Zhang, Q., Liang, K., and Liu, C.: Investigation of factors affecting
778 inter-annual variability of evapotranspiration and streamflow under different climate conditions.
779 *J. Hydrol.*, 543, 759-769, 2016.
- 780 Zhang, G., Xie, H., Yao, T., Liang, T., and Kang, S.: Snow cover dynamics of four lake basins
781 over Tibetan Plateau using time series MODIS data (2001-2100), *Water Resour. Res.*, 48(10),
782 W10529, 2012.
- 783 Zhang, K., Kimball, J.S., Nemani, R.R., and Running, S.W.: A continuous satellite-derived global
784 record of land surface evapotranspiration from 1983 to 2006, *Water Resour. Res.*, 46(9),
785 W09522, 2010.
- 786 Zhang, L., Su, F., Yang, D., Hao, Z., and Tong, K.: Discharge regime and simulation for the
787 upstream of major rivers over Tibetan Plateau, *J. Geophys. Res. Atmos.*, 118(15), 8500-8518,
788 2013.
- 789 Zhang, Q., Li, J., Singh, V., and Xu, C.: Copula-based spatial-temporal patterns of precipitation
790 extremes in China, *Int. J. Climatol.*, 33, 1140-1152, 2013.
- 791 Zhang, X., Tang, Q., Pan, M., and Tang, Y.: A long-term land surface hydrologic fluxes and states
792 dataset for China, *J. Hydrometeorol.*, 15, 2067-2084, 2014.
- 793 Zhang, Y., Peña-Arancibia, J.L., McVicar, T.R., Chiew, F.H.S., Vaze, J., Liu, C.M., Lu, X.J.,
794 Zheng, H.X., Wang, Y.P., Liu, Y.Y., Miralles, D.G., and Pan, M.: Multi-decadal trends in global
795 terrestrial evapotranspiration and its components, *Scientific Reports*, 6, 19124, 2016.
- 796 Zhang, Y., Liu, C., Tang, Y., and Yang, Y.: Trend in pan evaporation and reference and actual
797 evapotranspiration across the Tibetan Plateau, *J. Geophys. Res.*, 112, D12110, 2007.



- 798 Zhou, C., Jia, S., Yan, H., and Yang, G.: Changing trend of water resources in Qinghai Province
799 from 1956 to 2000, *J. Glaciol. Geocryol.*, 27(3), 432-437, 2005 (in Chinese).
- 800 Zhou, J., Wang, L., Zhang, Y.S., Guo, Y.H., Li, X.P., and Liu, W.B.: Exploring the water storage
801 changes in the largest lake (Selin Co) over the Tibetan Plateau during 2003-2012 from a
802 basin-wide hydrological modeling., *Water Resour. Res.*, 51, 8060-8086, 2015.
- 803 Zhou, S.Q., Kang, S., Chen, F., and Joswiak, D.R.: Water balance observations reveal significant
804 subsurface water seepage from Lake Nam Co., south-central Tibetan Plateau., *J. Hydrol.*, 491,
805 89-99, 2013.
- 806 Zhu, Y., Chen, J., Chen, G.: Runoff variation and its impacting factors in the headwaters of the
807 Yangtze River in recent 32 years, *J. Yangtze River Sci. Res. Inst.*, 28(6), 1-4, 2011 (in Chinese).



Table 1: Overview of multi-source datasets applied in this study

Data category	Data source	Spatial resolution	Temporal resolution	Available period used	Reference
Runoff (Q)	Observed, National Hydrology Almanac of China	—	Daily	1982-2011	—
Precipitation (P)	VIC_IGSNRR simulated	0.25°	Daily	1982-2011	Zhang et al. (2014)
	Observed, CMA	0.5°	Monthly	1982-2011	—
	TRMM 3B43 V7	0.25°	Monthly	2000-2011	Huffman et al. (2012)
	IGSNRR forcing	0.25°	Daily	1982-2011	Zhang et al. (2014)
Temperature (Temp.)	Observed, CMA	0.5°	Monthly	2000-2011	—
Terrestrial storage change (ΔS)	GRACE-CSR	Approx. 300-400 km	Monthly	2002-2011	Tapley et al. (2004)
	GRACE-GFZ	Approx. 300-400 km	Monthly	2002-2011	Tapley et al. (2004)
	GRACE-JPL	Approx. 300-400 km	Monthly	2002-2011	Tapley et al. (2004)
Potential evaporation (PET)	CRU	0.5°	Monthly	1982-2011	Harris et al. (2013)
Actual evaporation (ET)	MTE_E	0.5°	Monthly	1982-2011	Jung et al. (2010)
	VIC_E	0.25°	Daily	1982-2011	Zhang et al. (2014)
	GLEAM_E	0.25°	Daily	1982-2011	Miralles et al. (2011)
	PML_E	0.5°	Monthly	1982-2011	Zhang Y et al. (2016)
	Zhang_E	8 km	Monthly	1983-2006	Zhang et al. (2010)
	GNoah_E	1.0°	3 hourly	1982-2011	Rui (2011)
NDVI	GIMMS NDVI dataset	8 km	15 daily	1982-2011	Tucker et al. (2005)
LAI	GLASS LAI Product	0.05°	8 daily	1982-2011	Liang and Xiao (2012)
Snow Cover	TP Snow composite Products	500 m	Daily	2005-2013	Zhang et al. (2012)
SWE	VIC_IGSNRR simulated	0.25°	Daily	1982-2011	Zhang et al. (2014)
	GlobSnow-2 Product	25 km	Daily	1982-2011	Takala et al. (2011)
Glacier Area	the Second Glacier Inventory Dataset of China	—	—	2005	Guo et al. (2014)



Table 2: Main features of the 18 TP river basins used in this study. The precipitation and temperature statistics for each basin were calculated from the observed CMA datasets while the NDVI and LAI statistics were extracted from the GIMMS NDVI dataset and GLASS LAI product. The GA% and SC% represented the percentages of multiyear-mean glacier cover and snow cover in each basin which were calculated from the Second Glacier Inventory Dataset of China and the daily TP snow cover dataset (2005-2013)

No.	Station	Altitude (m)	River name	Drainage area (km ²)	Multiyear-mean (1982-2011) and basin-averaged parameters						
					Q (mm/yr)	Prec. (mm/yr)	Temp. (°C/yr)	NDVI	LAI	GA%	SC%
01	Kulukelangan	2000	Yerqiang	32880.00	158.60	128.34	-5.68	0.05	0.03	10.97	35.03
02	Tongguziluoke	1650	Yulongkashi	14575.00	151.56	134.04	-4.07	0.06	0.04	23.27	35.95
03	Numaitilangan	1880	Keliya	7358.00	103.18	137.14	-4.78	0.06	0.03	10.86	29.16
04	Zelingou	4282	Bayin	5544.00	41.42	340.68	-4.98	0.13	0.09	0.09	21.22
05	Gadatan	3823	Yellow	7893.00	200.95	566.01	-4.60	0.34	0.54	0.13	14.94
06	Xining	3225	Yellow	9022.00	99.90	503.74	0.97	0.36	0.70	0.00	10.06
07	Tongren	3697	Yellow	2832.00	149.36	533.25	-1.37	0.39	0.83	0.00	9.42
08	Tainaihai	2632	Yellow	121972.00	159.48	540.32	-2.40	0.34	0.72	0.09	15.89
09	Huangheyan	4491	Yellow	20930.00	31.18	386.42	-4.81	0.23	0.61	0.00	17.25
10	Jimai	4450	Yellow	45015.00	85.50	441.48	-4.16	0.26	0.52	0.00	20.05
11	Yajiang	2599	Yalong	67514.00	237.66	717.05	-0.23	0.43	0.80	0.15	18.36
12	Zhimenda	3540	Yangtze	137704.00	96.23	405.66	-4.83	0.20	0.26	0.96	17.87
13	Jiaoyuqiao	3000	Salween	72844.00	364.26	620.88	-1.89	0.29	0.44	2.02	23.73
14	Pangduo	5015	Brahmaputra	16459.00	348.31	544.59	-1.53	0.27	0.33	1.66	23.33
15	Tangjia	4982	Brahmaputra	20143.00	350.61	555.17	-1.89	0.27	0.34	1.39	21.83
16	Gongbuijiangda	4927	Brahmaputra	6417.00	586.96	692.06	-4.24	0.27	0.36	4.12	25.99
17	Nuxia	2910	Brahmaputra	191235.00	307.38	401.35	-0.73	0.22	0.25	1.90	13.50
18	Yangcun	3600	Brahmaputra	152701.00	163.25	349.91	-0.87	0.19	0.18	1.28	10.52



815 **Table 3:** Annual-averaged water storage changes (ΔS) in 18 TP basins derived from GRACE retrievals (2002-2013) from three different processing centers (CSR,
816 GFZ and JPL)
817

Basin	Water storage Change (ΔS ,mm)		
	CSR	GFZ	JPL
Kulukelangan	-0.16	-0.16	-0.00
Tongguziluo	0.10	0.10	0.28
Numaitilang	0.24	0.22	0.41
Zelingou	0.63	0.41	0.69
Gadatan	0.02	-0.24	-0.03
Xining	-0.08	-0.35	-0.14
Tongren	-0.13	-0.41	-0.21
Tainaihai	0.12	-0.16	0.10
Huangheyan	0.60	0.35	0.70
Jimai	0.41	0.15	0.48
Yajiang	-0.23	-0.50	-0.21
Zhimenda	0.57	0.38	0.78
Jiaoyuqiao	-1.00	-1.13	-0.79
Nuxia	-1.42	-1.44	-1.31
Pangduo	-1.21	-1.29	-1.02
Tangjia	-1.40	-1.46	-1.24
Gongbujiangda	-1.61	-1.67	-1.47
Yangcun	-1.33	-1.34	-1.21



Table 4: Nonparametric trends for different ET estimates during the period 1982–2006 detected by modified Mann-Kendall test, the bold number showed the detected trend is statistically significant at the 0.05 level

Basin	ET _{wb}	GLEAM_E	VIC_E	Zhang_E	PML_E	MET_E	GNoah_E
Kulukelangan	-0.09	0.09	0.18	–	0.03	-0.01	0.07
Tongguziluoke	-0.02	0.10	0.13	–	0.03	-0.08	0.19
Numaitilangan	0.04	0.10	0.14	–	0.14	-0.10	0.22
Zelingou	0.13	0.23	0.11	0.09	0.04	0.06	0.02
Gadatan	-0.09	0.25	0.070	-0.10	-0.01	0.06	-0.07
Xining	-0.06	0.54	0.01	-0.08	0.01	0.02	-0.06
Tongren	-0.06	0.34	-0.15	-0.17	0.07	0.02	0.13
Tainaihai	0.06	0.28	-0.03	-0.11	0.04	0.05	0.04
Huangheyan	0.08	0.19	-0.01	-0.10	0.08	0.05	0.10
Jimai	-0.07	0.23	-0.01	-0.08	0.03	0.05	0.10
Yajiang	0.17	0.26	0.06	-0.21	-0.01	0.03	-0.02
Zhimenda	0.11	0.28	0.10	0.01	0.07	0.04	0.07
Jiaoyuqiao	0.18	0.28	0.10	-0.11	0.05	0.05	0.07
Nuxia	-0.09	0.25	0.09	-0.10	0.12	0.04	0.10
Pangduo	0.05	0.28	0.17	-0.07	0.07	0.07	0.11
Tangjia	0.09	0.26	0.17	-0.09	0.20	0.06	0.12
Gongbujiangda	-0.26	0.12	0.13	-0.16	0.19	0.01	0.15
Yangcun	0.03	0.28	0.08	-0.06	0.10	0.04	0.09



835 **Figure captions:**

836 **Figure 1.** Map of river basins and hydrological gauging stations (green dots) over the
 837 Tibetan Plateau (TP) used in this study. The grey shading shows the topography of TP
 838 in meters above the sea level and the blue shading exhibits the glaciers distribution in
 839 TP extracted from the Second Glacier Inventory Dataset of China.

840 **Figure 2.** Comparison of VIC_IGSNRR simulated and observed monthly runoff for
 841 Tangnaihai and Panduo stations (a and b) as well as (c) basin-averaged monthly
 842 TRMM, CMA gridded and IGSNRR forcing precipitations for the smallest basin
 843 (Tongren station) over the period 1982-2011. (d) shows the comparison of TRMM
 844 (blue) and IGSNRR forcing (red) precipitations against CMA gridded precipitation for
 845 18 river basins over TP during the period 2000-2011.

846 **Figure 3.** Comparison of different ET products against the calculated ET through the
 847 water balance method (ET_{wb}) at the monthly time scale for 18 TP basins during the
 848 period 1983-2006. The boxplot of monthly estimates of different ET products for 18
 849 TP basins are shown in (a) while the correlation coefficients and
 850 root-mean-square-errors (RMSEs, mm/month) for each ET product relatively to ET_{wb}
 851 are exhibited in (b).

852 **Figure 4.** General water and energy status (a. the perspective of Budyko framework)
 853 and their relationships with glacier (b) and vegetation (c and d) for eighteen TP river
 854 basins (1983-2006). The ET used in this figure is calculated from the bias-corrected
 855 water balance method.

856 **Figure 5.** Seasonal cycles (1982-2011) of water budget components in westerlies-
 857 dominated (column 1), East Asian monsoon-dominated (columns 2-4) and Indian
 858 monsoon-dominated (columns 5-6) TP basins.

859 **Figure 6.** Seasonal cycles (1982-2011) of air temperature and vegetation parameters
 860 in westerlies-dominated (column 1), East Asian monsoon-dominated (columns 2-4)
 861 and Indian monsoon-dominated (columns 5-6) TP basins.

862 **Figure 7.** Seasonal cycles (1982-2011) of snow cover and snow water equivalent
 863 (SWE) in westerlies-dominated (column 1), East Asian monsoon-dominated (columns



864 2-4) and Indian monsoon-dominated (columns 5-6) TP basins. The snow cover was
865 extracted from cloud free snow composite product during the period 2005-2013. It
866 should also be noted that the GlobSnow data are not available for some basins.

867 **Figure 8.** Sen's slopes of water budget components and vegetation parameters in
868 westerlies-dominated TP basins during the period of 1982-2011. To clearly exhibit the
869 nonparametric trends of all variables in one panel, the Sen's Slopes of Q , P , ET_{wb} and
870 PET have been multiplied by $1/12$ (unit: mm/month). The double red stars showed
871 that the trend was statistically significant at the 0.05 level.

872 **Figure 9.** Linear and non-parametric trends of westerly, Indian monsoon and East
873 Asian summer monsoon during the period 1982-2011 revealed prospectively by the
874 Asian Zonal Circulation Index, Indian Ocean Dipole Mode Index and East Asian
875 Summer Monsoon Index.

876 **Figure 10.** Similar to Figure 8 but for East Asian monsoon-dominated TP basins. It
877 should be noted that the GlobSnow data are not available for some basins. The double
878 red stars showed that the trend was statistically significant at the 0.05 level.

879 **Figure 11.** Similar to Figure 8 but for Indian monsoon-dominated TP basins. It should
880 be noted that the GlobSnow data are not available for some basins. The double red
881 stars showed that the trend was statistically significant at the 0.05 level.

882 **Figure 12.** Uncertainties in seasonal cycles of ET_{wb} calculated from three precipitation
883 products (CMA gridded, IGSNRR_Forcing and TRMM precipitation) in 18 TP basins.
884 The comparisons were conducted during the period 2000-2011 when TRMM data was
885 available.

886 **Figure 13.** Uncertainties in annual trends of ET_{wb} (b) calculated from two precipitation
887 products (CMA gridded and IGSNRR_Forcing) (a) in 18 TP basins. The comparisons
888 were conducted during the period 1982-2011 (TRMM data was not available for the
889 whole period).



Figure 1. Map of river basins and hydrological gauging stations (green dots) over the Tibetan Plateau (TP) used in this study. The grey shading shows the topography of TP in meters above the sea level and the blue shading exhibits the glaciers distribution in TP extracted from the Second Glacier Inventory Dataset of China.

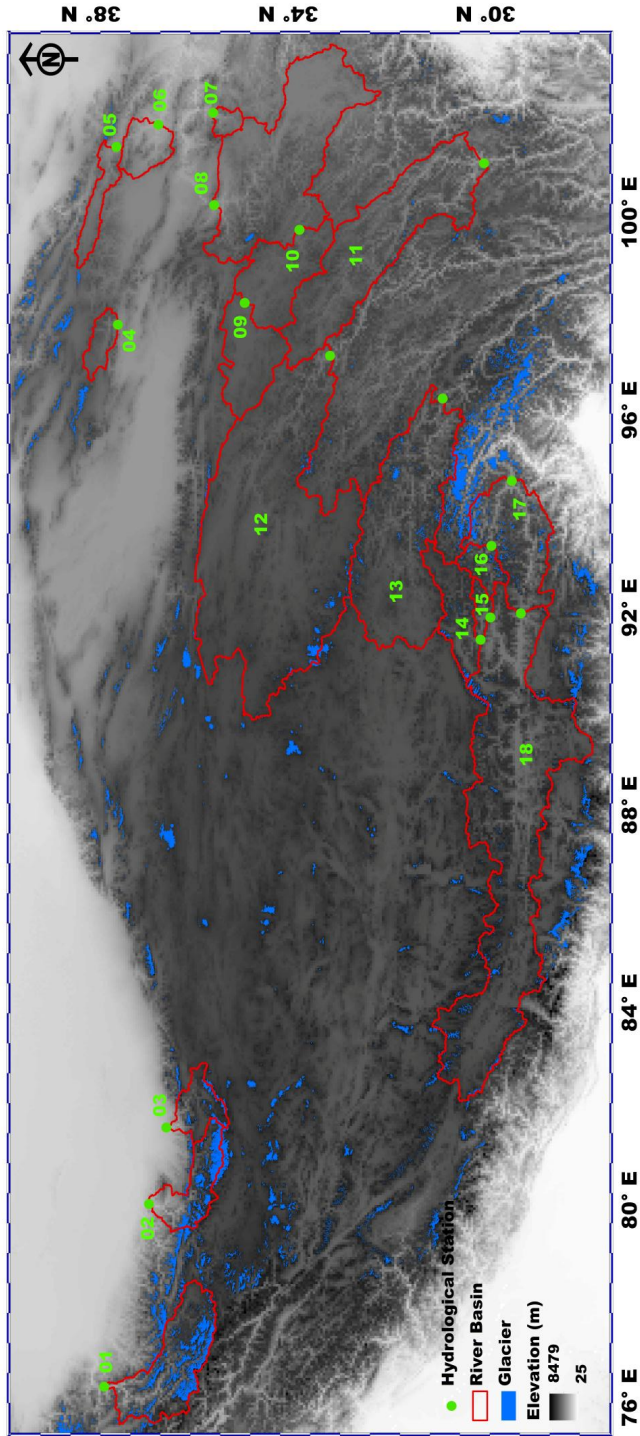




Figure 2. Comparison of VIC_IGSNRR simulated and observed monthly runoff for Tangnaihai and Panduo stations (a and b) as well as (c) basin-averaged monthly TRMM, CMA gridded and IGSNRR forcing for the smallest basin (Tongren station) over the period 1982-2011. (d) shows the comparison of TRMM (blue) and IGSNRR forcing (red) precipitations against CMA gridded precipitation for 18 river basins over TP during the period 2000-2011.

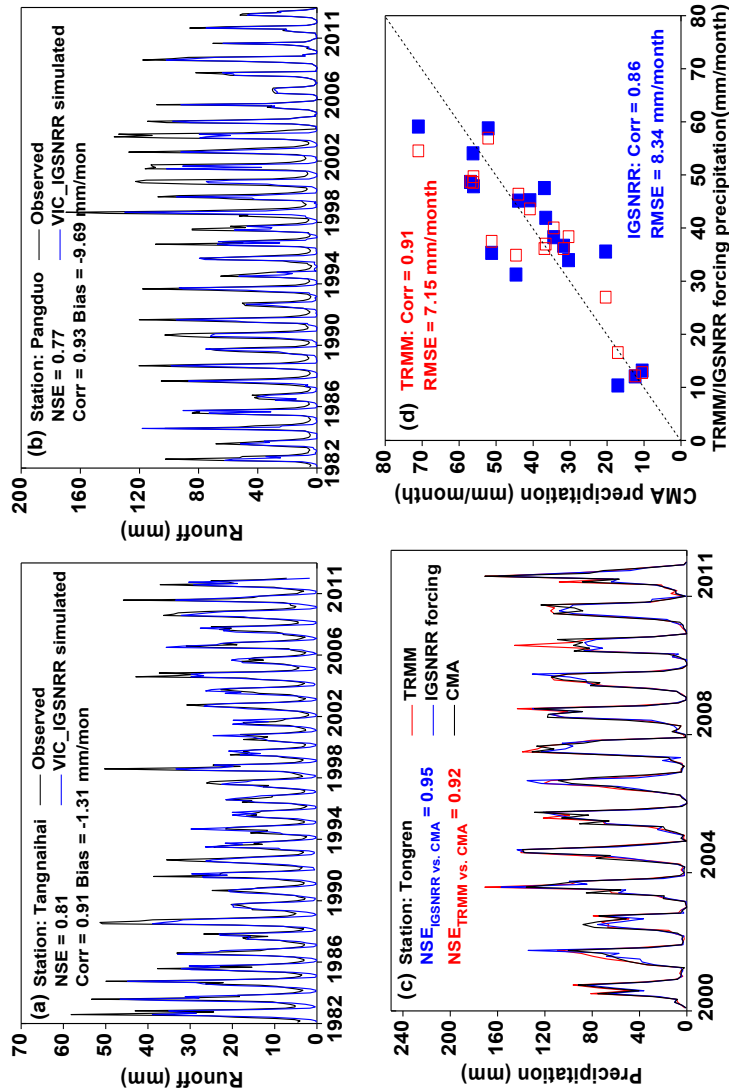




Figure 3. Comparison of different ET products against the calculated ET through the water balance (ET_{wb}) at the monthly time scale for 18 river basins over the Tibetan Plateau during the period 1983–2006. The boxplot of monthly estimates of different ET products for 18 TP basins are shown in (a) while the correlation coefficients and root-mean-square-errors (RMSEs, mm/month) for each ET product relatively to ET_{wb} are exhibited in (b).

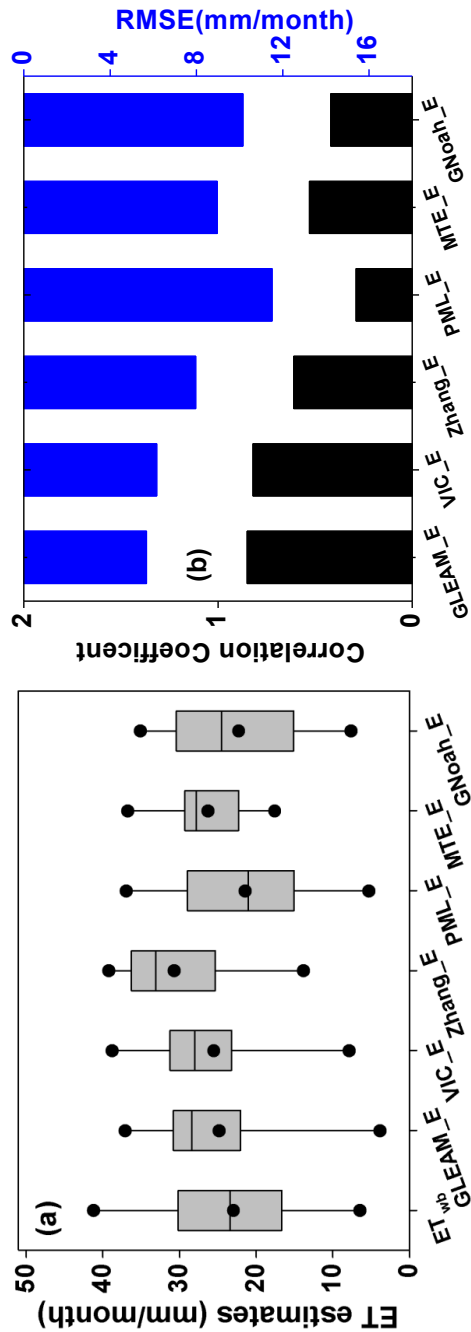




Figure 4. General water and energy status (a. the perspective of Budyko framework) and their relationships with glacier (b) and vegetation (c and d) for eighteen TP river basins (1983-2006). The ET used in this figure is calculated from the bias-corrected water balance method.

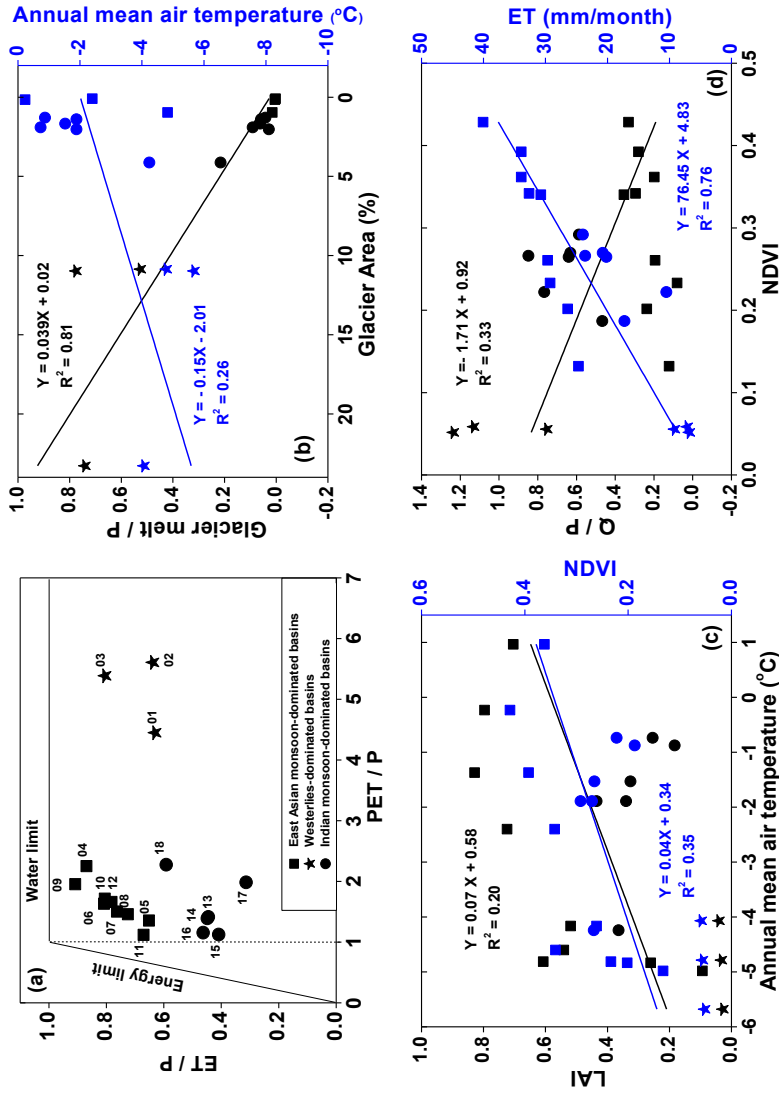




Figure 5. Seasonal cycles (1982–2011) of water budget components in westerlies-dominated (column 1), East Asian monsoon-dominated (columns 2–4) and Indian monsoon-dominated (columns 5–6) TP basins.

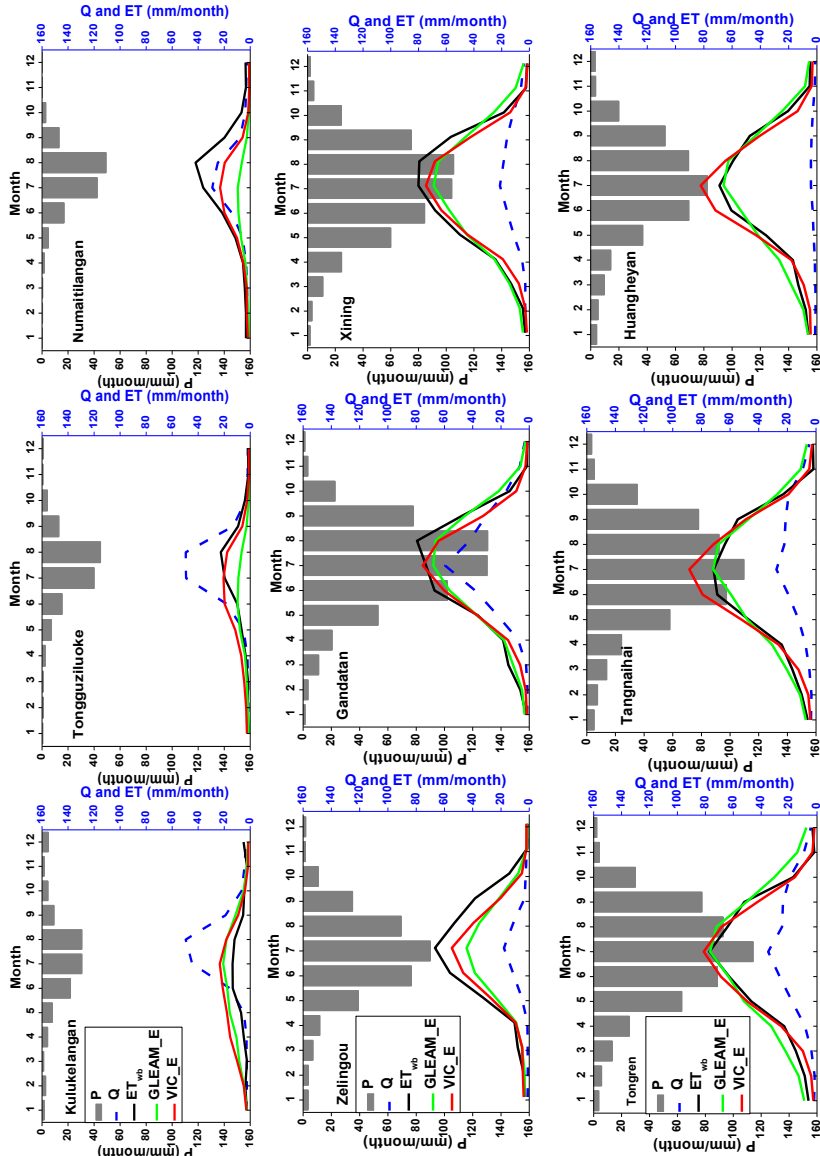
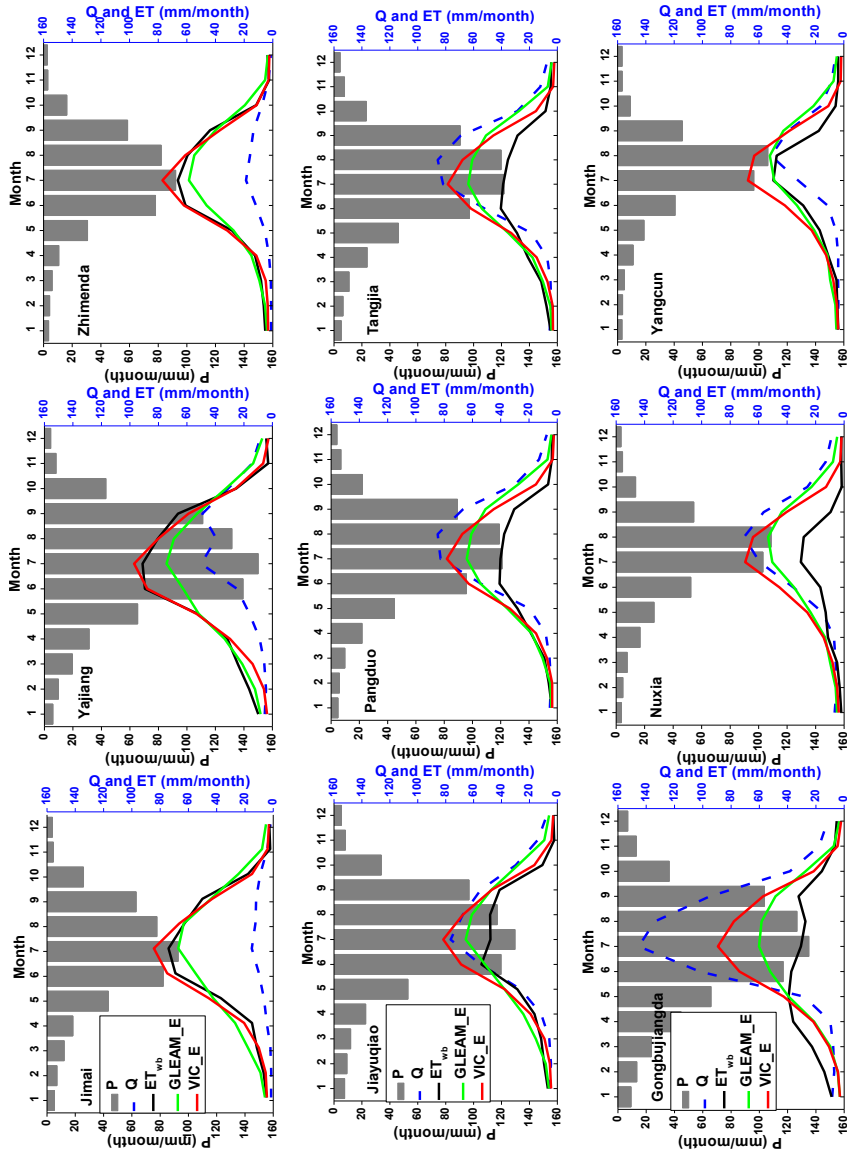




Figure 5: (continued)





919 **Figure 6.** Seasonal cycles (1982–2011) of air temperature and vegetation parameters in westerlies-dominated (column 1), East Asian monsoon-dominated (columns
920 2–4) and Indian monsoon-dominated (columns 5–6) TP basins.

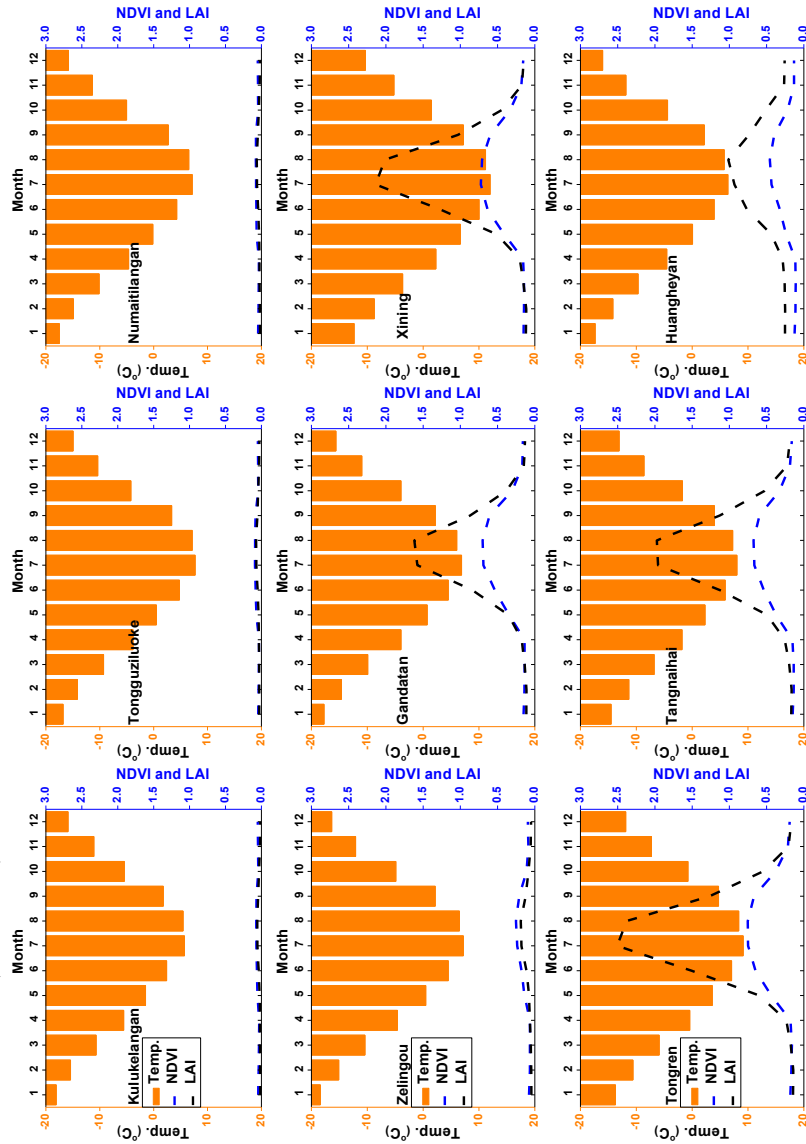
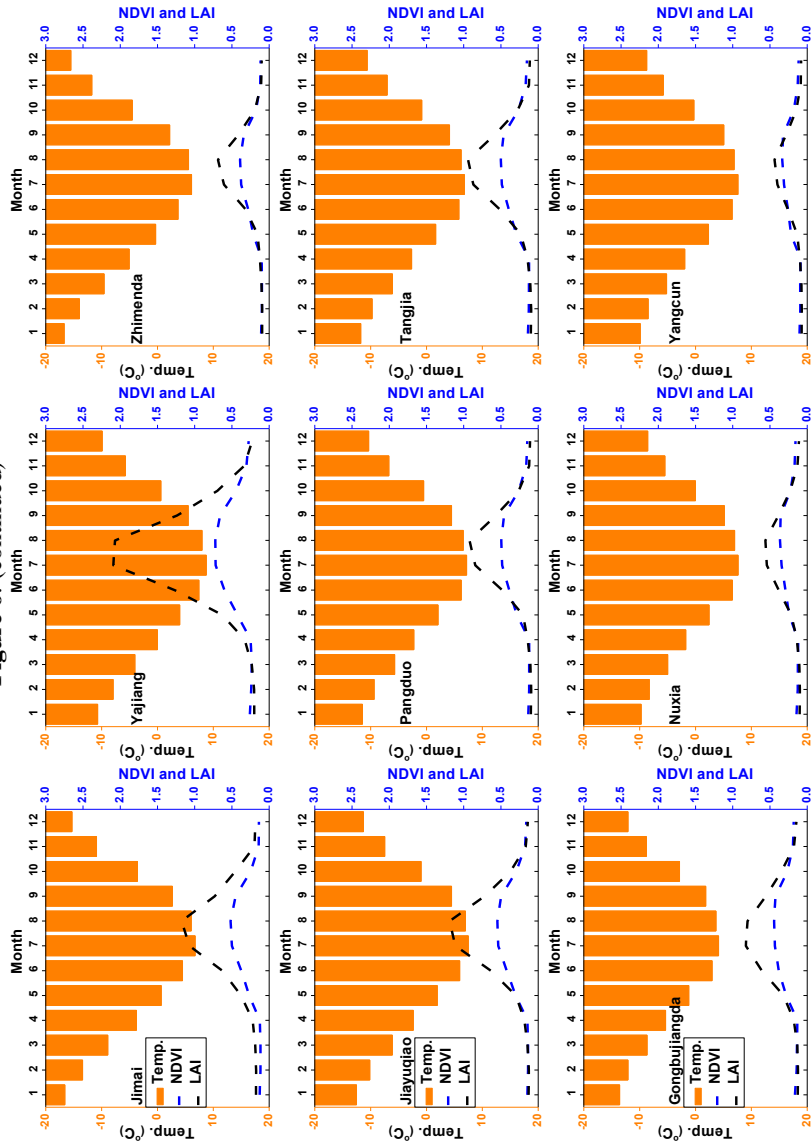




Figure 6: (continued)





929 **Figure 7.** Seasonal cycles (1982-2011) of snow cover and snow water equivalent (SWE) in westerlies-dominated (column 1), East Asian monsoon-dominated
930 (columns 2-4) and Indian monsoon-dominated (columns 5-6) TP basins. The snow cover was extracted from cloud free snow composite product during the period
931 2005-2013. It should also be noted that the GlobSnow data are not available for some basins.
932

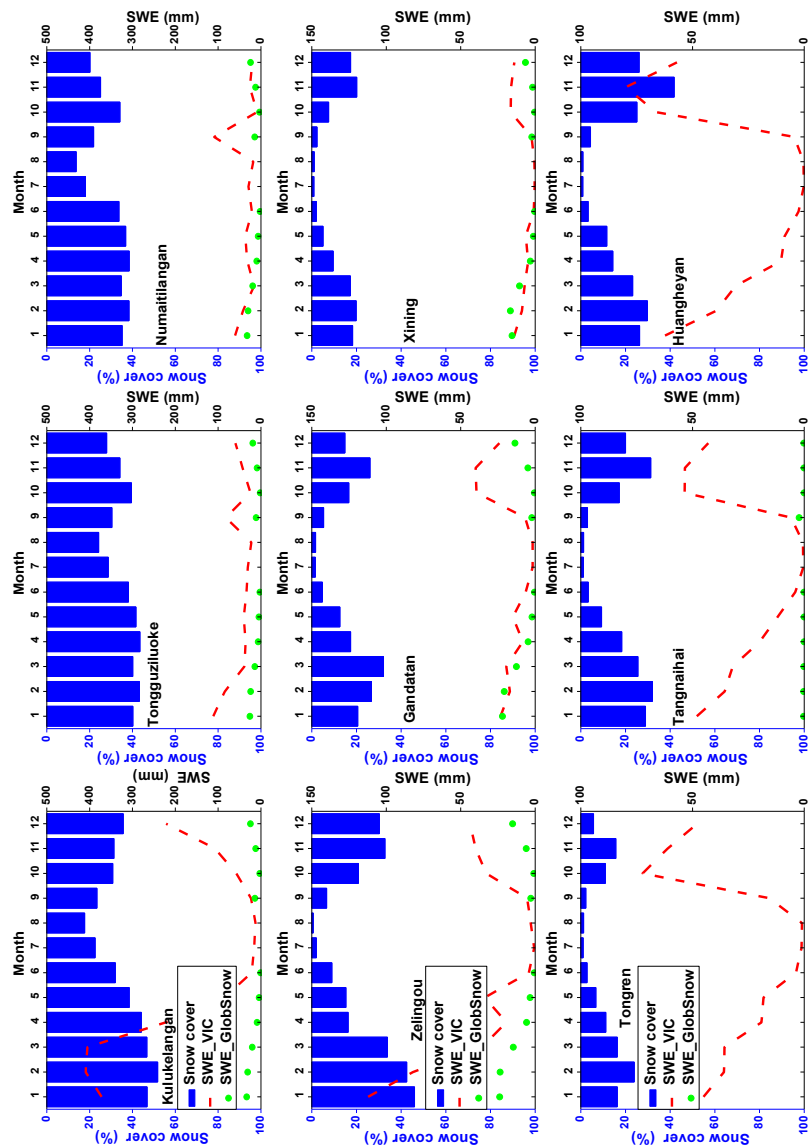




Figure 7: (continued)

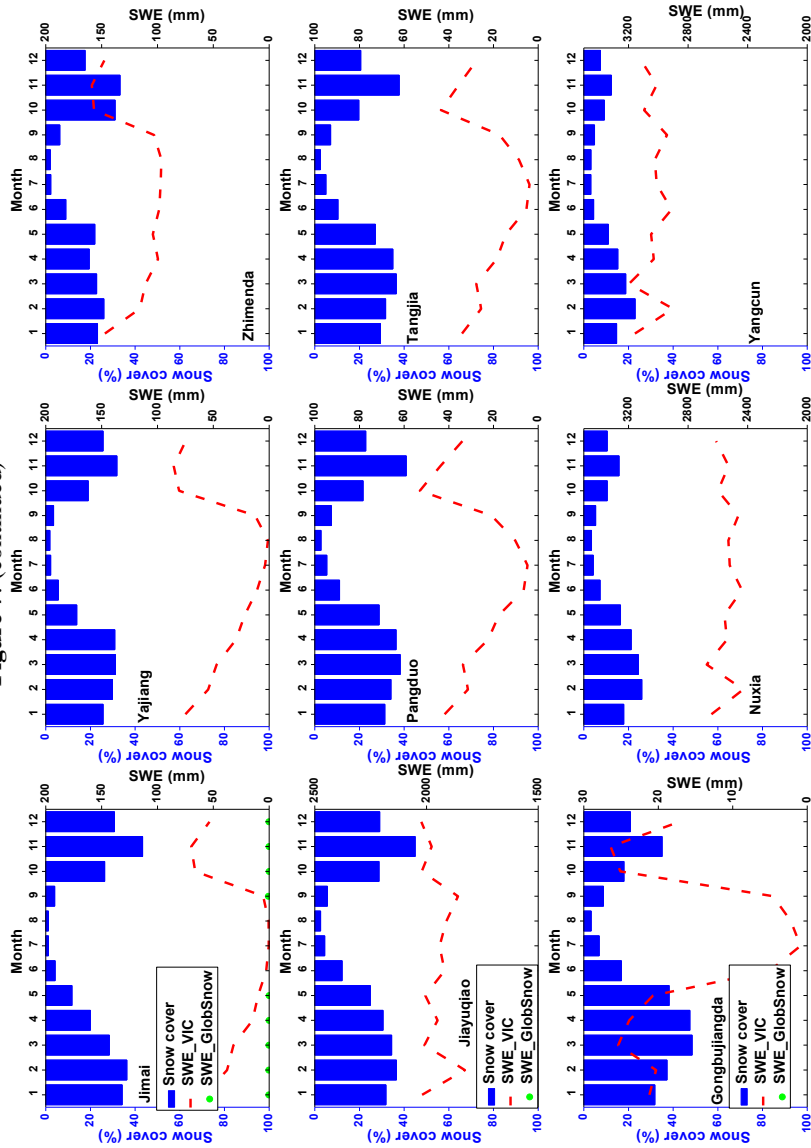




Figure 8. Sen's slopes of water budget components and vegetation parameters in westerlies-dominated TP basins during the period of 1982-2011. To clearly exhibit the nonparametric trends of all variables in one panel, the Sen's Slopes of Q, P, ET_{wb} and PET have been multiplied by 1/12 (unit: mm/month). The double red stars showed that the trend was statistically significant at the 0.05 level.

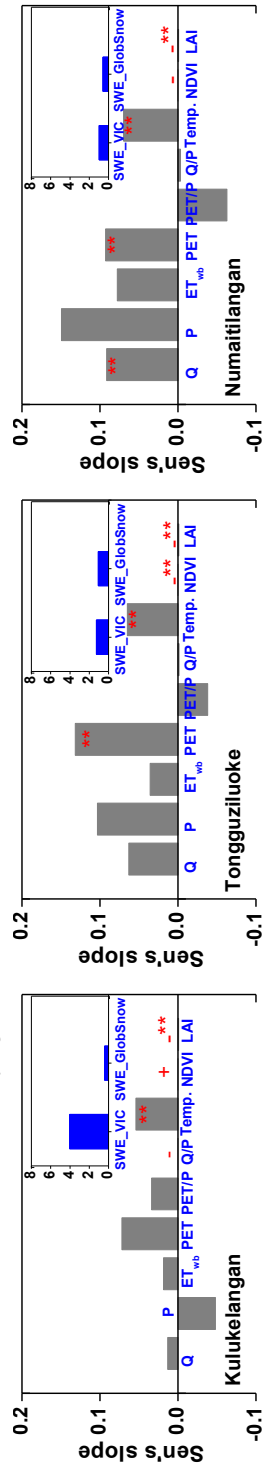




Figure 9. Linear and non-parametric trends of westerly, Indian monsoon and East Asian summer monsoon during the period 1982-2011 revealed prospectively by the Asian Zonal Circulation Index, Indian Ocean Dipole Mode Index and East Asian Summer Monsoon Index.

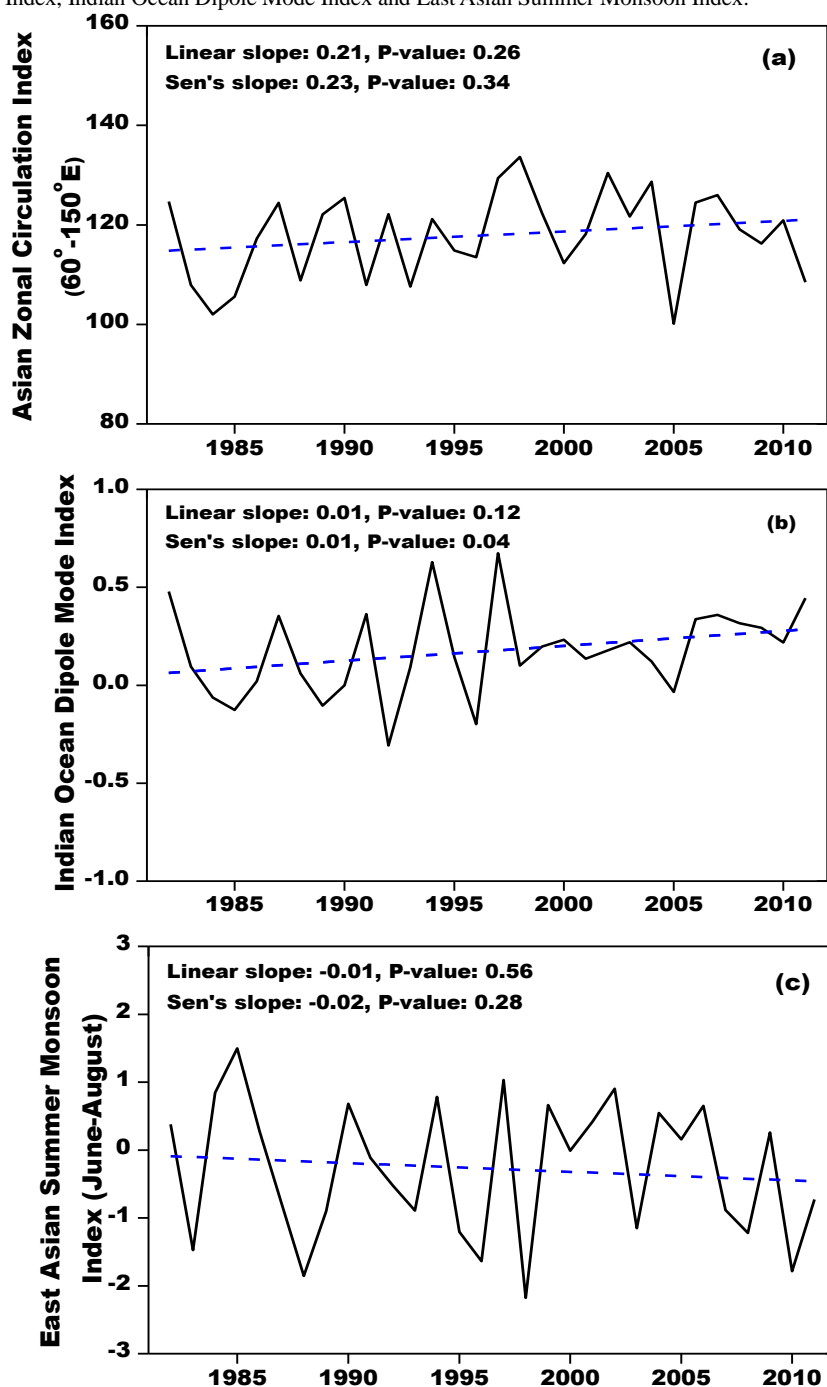




Figure 10. Similar to Figure 8 but for East Asian monsoon-dominated TP basins. It should be noted that the GlobSnow data are not available for some basins.

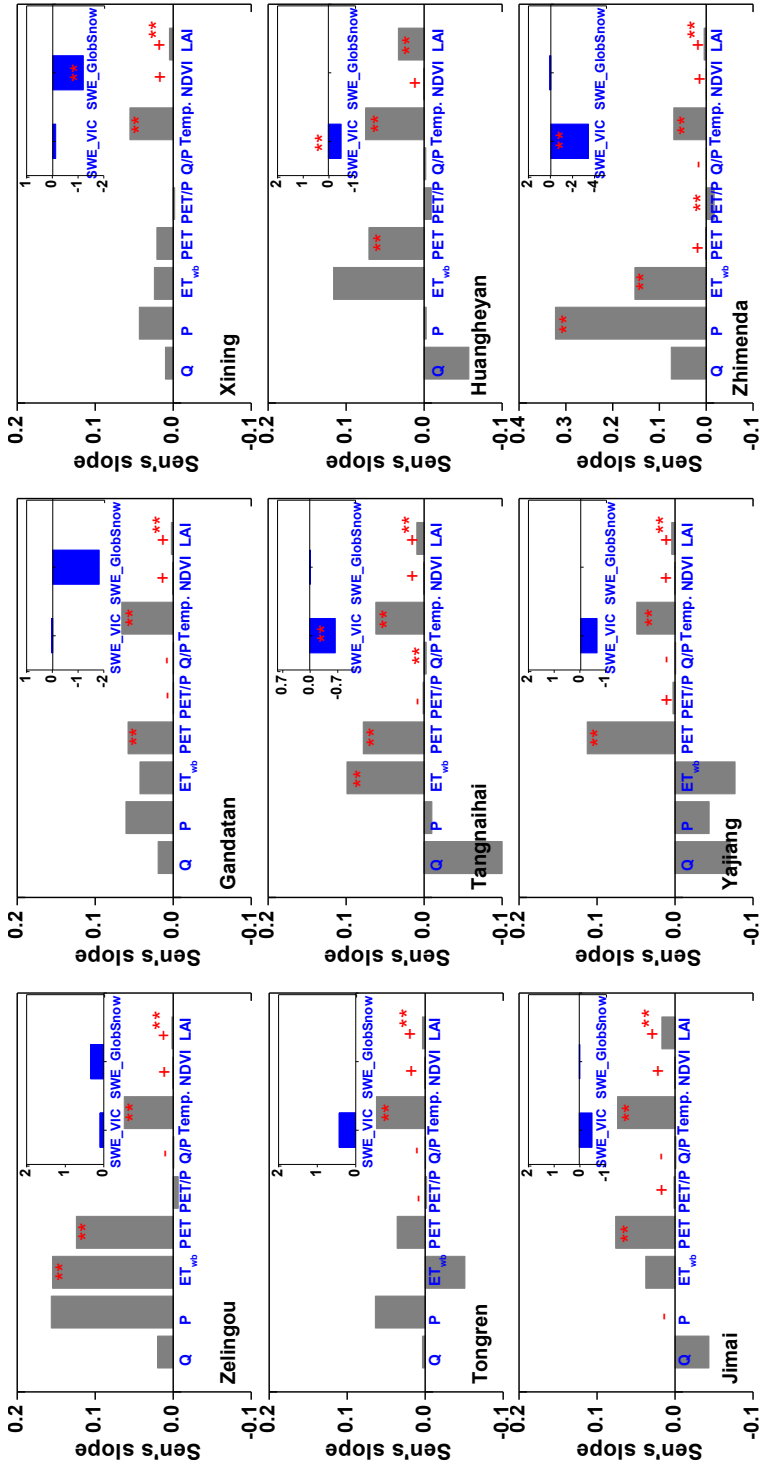




Figure 11. Similar to Figure 8 but for Indian monsoon-dominated TP basins. It should be noted that the GlobSnow data are not available for some basins.

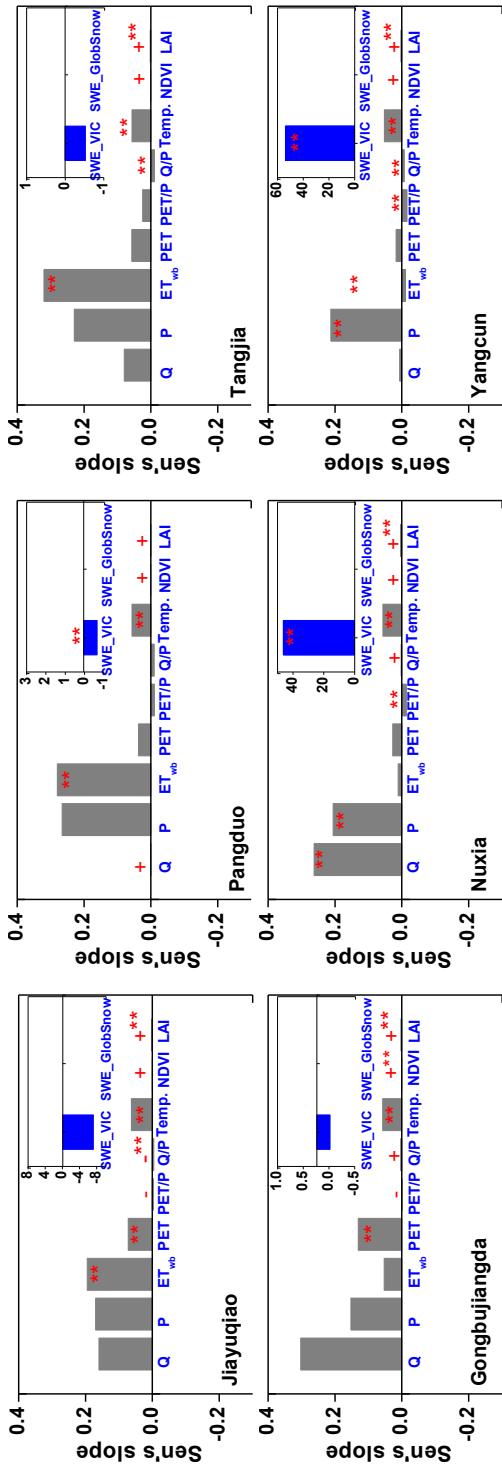




Figure 12. Uncertainties in seasonal cycles of ET_{wb} calculated from three precipitation products (CMA gridded, IGSNRR Forcing and TRMM precipitation) in 18 TP basins. The comparisons were conducted during the period 2000–2011 when TRMM data was available.

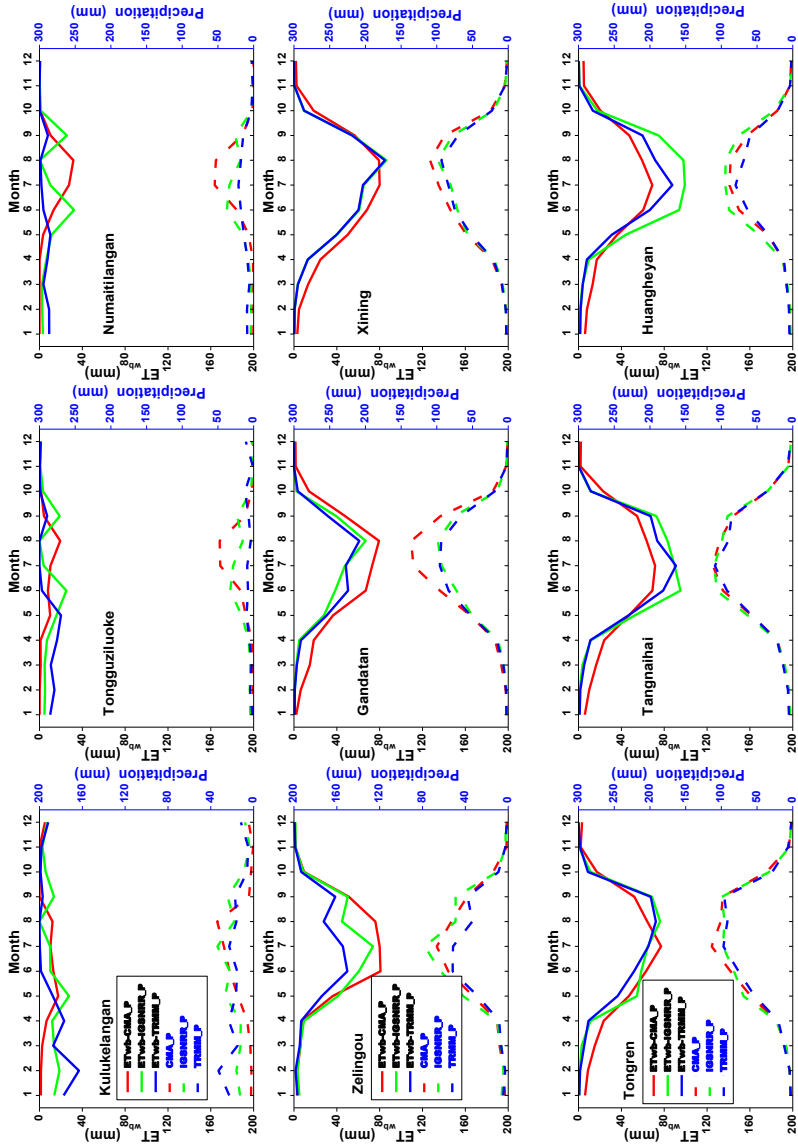




Figure 12: (continued)

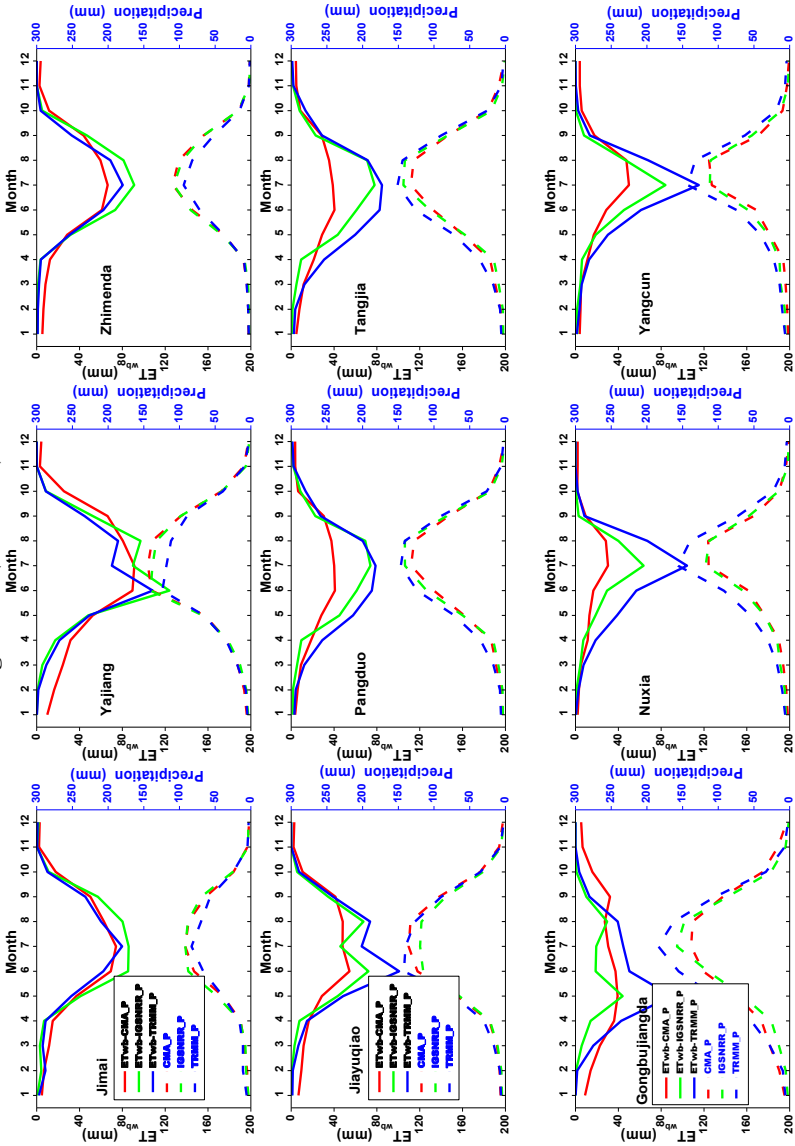




Figure 13. Uncertainties in annual trends of ET_{wb} (b) calculated from two precipitation products (CMA gridded and IGSNRR_Fforcing) (a) in 18 TP basins. The comparisons were conducted during the period 1982-2011 (TRMM data was not available for the whole period).

